

Q-BioLAT: Binary Latent Protein Fitness Landscapes for QUBO-Based Optimization

Truong-Son Hy

University of Alabama at Birmingham
Birmingham, Alabama, USA
thy@uab.edu

Abstract

Protein fitness optimization is inherently a discrete combinatorial problem, yet most learning-based approaches rely on continuous representations and are primarily evaluated through predictive accuracy. We introduce Q-BioLAT, a framework for modeling and optimizing protein fitness landscapes in compact binary latent spaces. Starting from pretrained protein language model embeddings, we construct binary latent representations and learn a quadratic unconstrained binary optimization (QUBO) surrogate that captures unary and pairwise interactions.

Beyond its formulation, Q-BioLAT provides a representation-centric perspective on protein fitness modeling. We show that representations with similar predictive performance can induce fundamentally different optimization landscapes. In particular, learned autoencoder-based representations collapse after binarization, producing degenerate latent spaces that fail to support combinatorial search, whereas simple structured representations such as PCA yield high-entropy, decodable, and optimization-friendly latent spaces.

Across multiple datasets and data regimes, we demonstrate that classical combinatorial optimization methods, including simulated annealing, genetic algorithms, and greedy hill climbing, are highly effective in structured binary latent spaces. By expressing the objective in QUBO form, our approach connects modern machine learning with discrete and quantum-inspired optimization.

Our implementation and dataset are publicly available at: <https://github.com/HySonLab/Q-BioLAT-Extended>.

Keywords: Protein Fitness Landscapes, Protein Language Models, Binary Latent Representations, QUBO Optimization, Combinatorial Optimization, Simulated Annealing, Quantum Annealing, Protein Engineering, Bioinformatics.

1 Introduction

Understanding and optimizing protein fitness landscapes is a central challenge in computational biology, with applications spanning enzyme engineering, drug discovery, and synthetic biology. Protein fitness landscapes are typically high-dimensional, rugged, and shaped by complex interactions between residues, making efficient exploration of sequence space difficult [1–3]. Recent advances in protein language models (PLMs), such as ESM-2 [4] and ESM-3

[5], have enabled powerful representations of protein sequences by learning from large-scale unlabeled data. These representations have significantly improved performance on downstream tasks, including mutation effect prediction [6, 7] and protein design [8–10].

Despite these advances, most existing approaches rely on continuous neural predictors and gradient-based [9] or sampling-based optimization strategies [10], which are not naturally suited for discrete combinatorial search. In particular, protein sequences are inherently discrete objects, and many biologically relevant optimization problems are fundamentally combinatorial in nature. Classical approaches such as evolutionary algorithms [10, 11] and Bayesian optimization [12, 13] have been widely applied to protein engineering, but they often struggle with scalability or require large numbers of evaluations. More importantly, existing methods primarily emphasize predictive accuracy, while the role of the underlying representation in shaping the *optimization landscape* remains underexplored.

In this work, we introduce Q-BioLAT, a framework that maps protein sequences into binary latent spaces where fitness landscapes can be explicitly modeled and optimized (see Figure 1). Starting from pretrained protein language model embeddings, we construct compact binary representations that enable the formulation of protein fitness as a quadratic unconstrained binary optimization (QUBO) [14–16] problem. This formulation transforms protein fitness modeling into a structured energy landscape over binary variables, allowing us to leverage a wide range of combinatorial optimization techniques, including simulated annealing and genetic algorithms, for efficient exploration of protein fitness landscapes.

Beyond its algorithmic formulation, Q-BioLAT provides a representation-centric perspective on protein fitness modeling through the lens of induced optimization landscapes. We show that representations with similar predictive performance can exhibit markedly different optimization behavior, as determined by the geometry of the latent space and the structure of the corresponding QUBO interactions. In particular, we observe a clear distinction between *prediction quality* and *optimization effectiveness*: learned autoencoder-based representations collapse after binarization, producing degenerate latent codes that fail to support combinatorial search, whereas simple structured representations such as

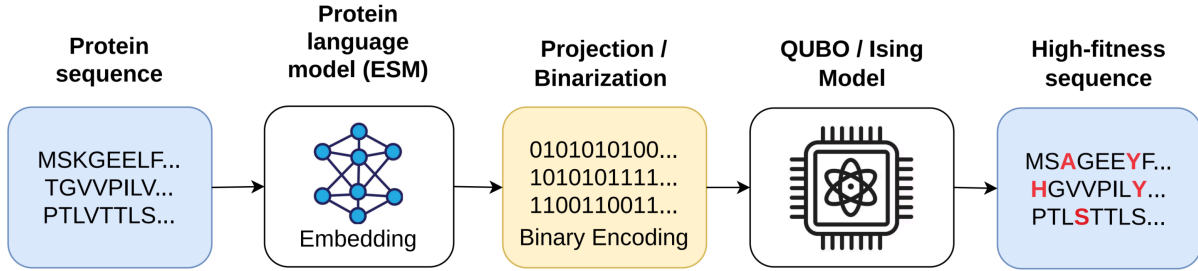


Figure 1. Overview of the Q-BioLAT framework. Protein sequences are first encoded using a pretrained protein language model (ESM) to obtain continuous embeddings. These embeddings are transformed into binary latent representations through projection and binarization, enabling protein fitness to be modeled as a quadratic unconstrained binary optimization (QUBO) problem. The resulting latent fitness landscape can be explored using combinatorial optimization methods and is directly compatible with quantum annealing hardware. Optimized latent codes are mapped back to high-fitness protein sequences.

PCA yield high-entropy and optimization-friendly latent spaces.

Empirically, we demonstrate that PCA-based binary latent representations consistently outperform both random projections and learned AE/VAE representations in decoding quality and end-to-end protein design performance across multiple datasets and data regimes. Furthermore, classical combinatorial optimization methods, including simulated annealing, genetic algorithms, and greedy hill climbing, are highly effective when applied to these structured latent landscapes, reliably identifying high-fitness regions even in data-scarce settings. We also observe that optimization performance depends on latent dimensionality, revealing a trade-off between expressivity, generalization, and searchability.

Overall, Q-BioLAT bridges protein language modeling, discrete latent representation learning, and combinatorial optimization by reframing protein fitness modeling as the construction of an optimization-aware energy landscape. By expressing protein fitness landscapes as QUBO problems, our framework provides a natural interface between modern machine learning models and discrete optimization methods, while also offering a pathway toward integration with quantum and quantum-inspired optimization paradigms.

2 Related Work

Protein language models and sequence representations. Recent advances in protein language models (PLMs) have significantly improved the representation of biological sequences by leveraging large-scale unlabeled protein data. Models such as ESM-2 [4] and its successor ESM-3 [5] learn contextual embeddings that capture structural and functional properties of proteins directly from sequence data. More recently, multimodal protein language models have been developed to integrate sequence information with additional modalities such as structure, function, and evolutionary context, further enhancing representation quality and downstream performance [17, 18]. These models have

demonstrated strong performance across a wide range of tasks, including structure prediction, mutation effect prediction, and protein design [19, 20]. In this work, we build upon PLM embeddings as a foundation, but transform them into binary latent representations to enable discrete optimization.

Protein fitness prediction and engineering. Predicting protein fitness landscapes is a fundamental problem in computational biology, with applications in enzyme optimization, therapeutic design, and synthetic biology. Recent approaches combine machine learning models with experimental data, particularly from deep mutational scanning (DMS) experiments, to predict the effects of mutations [21, 22]. Large-scale benchmarks such as ProteinGym have been introduced to systematically evaluate fitness prediction models across diverse proteins and mutation regimes [3]. While these methods achieve strong predictive performance, they typically rely on continuous representations and do not directly address the combinatorial nature of sequence optimization. Furthermore, these approaches primarily focus on prediction rather than explicitly enabling structured optimization over discrete sequence spaces.

Optimization methods for protein design. A variety of optimization strategies have been applied to protein engineering, including evolutionary algorithms [9–11, 13], Bayesian optimization [12, 13], and reinforcement learning [23, 24]. Evolutionary methods such as genetic algorithms are widely used due to their ability to explore large discrete search spaces, while Bayesian optimization offers sample-efficient search under expensive evaluation settings. Classical optimization techniques such as simulated annealing have also been applied to combinatorial problems with rugged energy landscapes [25, 26]. However, many of these approaches operate directly in sequence space or continuous embedding spaces, rather than explicitly modeling protein fitness as a structured combinatorial optimization problem. In contrast, our approach explicitly models protein fitness as a structured

combinatorial optimization problem in a learned binary latent space.

QUBO formulations and quantum annealing. Quadratic unconstrained binary optimization (QUBO) [14–16] provides a unified framework for expressing a wide range of combinatorial problems in terms of binary variables and pairwise interactions. QUBO formulations are closely related to the Ising model and form the basis of many optimization techniques, including quantum annealing [15]. Quantum annealing hardware, such as that developed by D-Wave Systems, has demonstrated the ability to solve certain classes of optimization problems by exploiting quantum effects [27]. While applications of quantum optimization in computational biology remain limited, recent work has begun to explore its potential for tasks such as molecular design and protein folding. In this work, we formulate protein fitness landscapes as QUBO problems in a binary latent space, enabling direct compatibility with both classical combinatorial solvers and emerging quantum annealing hardware, and providing a unified perspective on protein design as discrete energy landscape optimization.

Latent space optimization and discrete representations. Optimizing in learned latent spaces has become a common strategy in machine learning, particularly for generative modeling and design tasks [28, 29]. Continuous latent spaces have been widely used for molecule and protein generation [9, 30, 31], but they often require gradient-based optimization or sampling methods that do not naturally handle discrete constraints. More recently, discrete and binary latent representations have been explored for enabling combinatorial search and efficient optimization [32, 33]. Our work builds on this idea by constructing binary latent representations derived from protein language models and explicitly modeling the resulting fitness landscape as a QUBO problem, bridging representation learning and combinatorial optimization.

Energy landscapes and combinatorial optimization. Many combinatorial optimization problems can be interpreted through the lens of energy landscapes, where the objective function defines a surface over discrete configurations and optimization corresponds to navigating this landscape toward low-energy (or high-fitness) regions [34, 35]. In particular, QUBO formulations are closely related to Ising models and have been widely studied in statistical physics as models of interacting binary systems [15]. The structure of the interaction matrix determines key properties of the landscape, such as smoothness, ruggedness, and the distribution of local optima, which in turn strongly influence optimization difficulty [36, 37]. Such energy landscape perspectives have also been explored in machine learning, particularly

in the analysis of non-convex optimization and neural network loss surfaces [37, 38]. While these ideas are well established in physics and optimization, their role in modern representation learning pipelines for biological sequence design remains underexplored. In this work, we adopt an energy landscape view of protein fitness modeling in binary latent spaces and study how representation-induced structure affects combinatorial search.

Representation learning for optimization. Most existing representation learning approaches in protein modeling and related domains focus on improving predictive performance on downstream tasks, such as regression or classification [6, 7, 19]. However, in design and optimization settings, the learned representation implicitly defines a search space and induces an optimization landscape. Recent work in latent space optimization has explored how learned embeddings can facilitate search in applications such as molecule design, protein engineering, and combinatorial optimization [39–42]. These approaches typically leverage continuous latent spaces learned by variational autoencoders or related generative models, enabling gradient-based or sampling-based search. In protein design, similar ideas have been explored through latent generative models and language-model-guided optimization [8–10], where representations are used to guide exploration of sequence space. However, these approaches are primarily evaluated through predictive metrics, likelihood, or sample quality, rather than explicit analysis of the induced optimization landscape. More broadly, recent work in machine learning has begun to study how representations influence optimization and search behavior [43, 44], but this perspective remains underdeveloped in the context of biological sequence design. In contrast, our work emphasizes that representation quality should also be assessed based on the properties of the induced optimization landscape, and demonstrates that different representations with similar predictive accuracy can lead to substantially different optimization outcomes.

3 Method

3.1 Overview

We propose Q-BioLAT, a framework for modeling and optimizing protein fitness landscapes in a binary latent space. Given a protein sequence, Q-BioLAT first computes a pre-trained protein language model embedding, then transforms this continuous representation into a compact binary latent code. In this binary space, the fitness landscape is approximated by a quadratic unconstrained binary optimization (QUBO) surrogate, which models both unary and pairwise effects among latent variables. The learned surrogate is then optimized using combinatorial search methods such as simulated annealing and genetic algorithms. Because the final

objective is expressed in QUBO form, the framework is naturally compatible with both classical combinatorial solvers and quantum annealing hardware.

Formally, the overall pipeline is

$$s \rightarrow e(s) \in \mathbb{R}^d \rightarrow z(s) \in \mathbb{R}^m \rightarrow x(s) \in \{0, 1\}^m \rightarrow \hat{f}(x),$$

where s is a protein sequence, $e(s)$ is the protein language model embedding, $z(s)$ is a reduced continuous latent representation, $x(s)$ is the binarized latent code, and $\hat{f}(x)$ is the QUBO surrogate of protein fitness.

3.2 Problem Setup

Let $\mathcal{D} = \{(s_i, y_i)\}_{i=1}^N$ denote a protein fitness dataset, where s_i is a protein sequence and $y_i \in \mathbb{R}$ is its experimentally measured fitness. Our goal is to learn a surrogate model that maps each sequence to a compact binary latent representation and predicts its fitness, while also enabling efficient combinatorial optimization over the latent space.

Unlike conventional approaches that optimize directly in sequence space or in continuous embedding space, we aim to transform protein fitness prediction into a discrete optimization problem. This is motivated by two observations: first, protein sequences are inherently discrete objects; second, binary latent spaces admit efficient combinatorial search and can be directly mapped to QUBO and Ising formulations.

3.3 Protein Language Model Embeddings

For each protein sequence s_i , we obtain a continuous embedding using a pretrained protein language model. In our experiments, we use ESM-based sequence embeddings [4, 5] due to their strong empirical performance and broad adoption in protein representation learning. Given a sequence s_i of length L_i , the language model produces contextualized residue-level representations $H_i \in \mathbb{R}^{L_i \times d}$, where d is the hidden dimension of the model. To obtain a fixed-length sequence representation, we apply mean pooling across residues:

$$e_i = \frac{1}{L_i} \sum_{j=1}^{L_i} H_i^{(j)} \in \mathbb{R}^d.$$

This yields one dense embedding vector per sequence.

The role of the protein language model in Q-BioLAT is not to directly predict fitness, but rather to provide a biologically informed continuous representation that can later be compressed into a discrete latent code suitable for combinatorial optimization.

3.4 Continuous-to-Binary Latent Mapping

A key component of Q-BioLAT is the transformation of continuous protein embeddings into compact binary latent representations. While simple projection and thresholding provide a lightweight baseline, more expressive representations can be obtained by learning the latent mapping in a data-driven manner. In this work, we consider a unified family

of approaches for constructing binary latent codes, ranging from linear projections to learned autoencoding models.

Linear projection and binarization. Given a protein embedding $e \in \mathbb{R}^d$, we first consider linear dimensionality reduction methods such as random projection or principal component analysis (PCA):

$$z = We, \quad W \in \mathbb{R}^{m \times d}, \quad (1)$$

where $m \ll d$ is the latent dimension. The resulting continuous latent vector $z \in \mathbb{R}^m$ is then binarized using a thresholding function:

$$x_k = \mathbb{I}(z_k > \tau_k), \quad (2)$$

where τ_k is typically chosen as the median of the k -th component over the training set. This approach provides a simple and efficient baseline for constructing binary latent representations.

Deterministic binary autoencoder. To learn a more structured latent representation, we introduce a deterministic autoencoder [45, 46] that maps protein embeddings into a low-dimensional latent space and reconstructs them:

$$z = f_\theta(e), \quad \hat{e} = g_\phi(z), \quad (3)$$

where f_θ and g_ϕ denote the encoder and decoder networks, respectively. To obtain binary latent codes, we apply a binarization function:

$$x = \text{bin}(z), \quad (4)$$

where $\text{bin}(\cdot)$ may be implemented using thresholding or a sign function. The model is trained to minimize reconstruction loss:

$$\mathcal{L}_{\text{AE}} = \|e - \hat{e}\|_2^2. \quad (5)$$

This formulation allows the latent space to adapt to the structure of protein embeddings, potentially leading to more meaningful and optimization-friendly representations.

Variational latent representations. We further consider a probabilistic formulation based on variational autoencoders (VAEs) [47], which model a distribution over latent variables:

$$z \sim q_\theta(z | e), \quad \hat{e} \sim p_\phi(e | z). \quad (6)$$

The model is trained by maximizing the evidence lower bound (ELBO):

$$\mathcal{L}_{\text{VAE}} = \mathbb{E}_{q_\theta(z|e)} [\log p_\phi(e | z)] - \text{KL}(q_\theta(z | e) \| p(z)). \quad (7)$$

Binary latent codes can be obtained by applying a threshold or sampling from a Bernoulli distribution parameterized by the latent variables:

$$x_k \sim \text{Bernoulli}(\sigma(z_k)). \quad (8)$$

This probabilistic formulation enables modeling uncertainty in the latent representation and provides a principled way to explore the latent space.

Discussion. These approaches define different ways of constructing binary latent spaces, ranging from simple linear projections to learned deterministic and probabilistic mappings. Importantly, the choice of latent representation directly affects the structure of the induced QUBO model and, consequently, the geometry of the resulting optimization landscape. In Section 4, we empirically investigate how these different constructions influence both predictive performance and optimization behavior.

3.5 QUBO Surrogate for Protein Fitness

We model protein fitness in binary latent space with a QUBO surrogate. Given a binary latent code $x \in \{0, 1\}^m$, the predicted fitness is:

$$\hat{f}(x) = \sum_{k=1}^m h_k x_k + \sum_{1 \leq k < \ell \leq m} J_{k\ell} x_k x_\ell,$$

where $h_k \in \mathbb{R}$ captures the unary contribution of latent bit k , and $J_{k\ell} \in \mathbb{R}$ captures the pairwise interaction between bits k and ℓ . Equivalently, the model can be written in matrix form as:

$$\hat{f}(x) = h^\top x + \frac{1}{2} x^\top J x,$$

where $J \in \mathbb{R}^{m \times m}$ is the symmetric Hamiltonian (i.e. pairwise interaction matrix) with zero diagonal, and $h \in \mathbb{R}^m$ corresponds to the bias term. This representation connects the latent fitness model to the classical QUBO formulation.

Feature construction. For each binary code x_i , we construct a feature vector consisting of:

- all linear terms $\{x_{ik}\}_{k=1}^m$,
- all pairwise interaction terms $\{x_{ik}x_{i\ell}\}_{1 \leq k < \ell \leq m}$.

The total number of features is therefore:

$$m + \frac{m(m-1)}{2}.$$

Parameter estimation. We fit the QUBO surrogate using ridge regression. Let $\Phi(X)$ denote the design matrix formed by the linear and pairwise features of the training binary codes, and let y denote the corresponding fitness vector. We solve:

$$w^* = \arg \min_w \|\Phi(X)w - y\|_2^2 + \lambda \|w\|_2^2,$$

where $\lambda > 0$ is an ℓ_2 regularization coefficient. The learned parameter vector w^* is then unpacked into the unary coefficients h and pairwise coefficients J .

This surrogate is attractive for three reasons. First, it is interpretable, since each term corresponds to a unary or pairwise latent effect. Second, it is computationally efficient to fit and evaluate for moderate latent dimensions. Third, it directly yields a QUBO objective suitable for classical and quantum combinatorial optimization.

3.6 Latent Space Optimization

Once the QUBO surrogate has been fitted, we seek binary latent codes that maximize the predicted fitness:

$$x^* = \arg \max_{x \in \{0,1\}^m} \hat{f}(x).$$

Because this is a discrete combinatorial problem, we employ search strategies that operate directly in the binary latent space.

Simulated annealing [25]. Simulated annealing starts from an initial latent code and iteratively proposes single-bit flips. Moves that improve the objective are accepted, while worse moves may be accepted with a temperature-dependent probability, enabling escape from local optima. The temperature is gradually reduced during the search.

Genetic algorithm [26]. The genetic algorithm maintains a population of binary latent codes and evolves them through selection, crossover, and mutation. This allows broader exploration of the latent space and is particularly useful in higher-dimensional settings where multiple promising regions may exist.

Baselines. To contextualize performance, we also compare against greedy hill climbing, random search, and a lightweight latent Bayesian-style search baseline. Greedy hill climbing iteratively flips the single bit that most improves the objective until convergence. Random search samples binary codes uniformly and retains the best candidate. The latent Bayesian-style method uses a kernel-based uncertainty heuristic over binary latent codes.

3.7 Decoding of Optimized Latent Representations

A key step in Q-BioLAT is mapping optimized binary latent codes back to valid protein sequences. Since optimization is performed in latent space, decoding provides the connection between combinatorial search and biologically meaningful sequences.

Retrieval-based decoding. As a conservative baseline, we first use nearest-neighbor retrieval in Hamming space. Given an optimized latent code, we identify the closest latent codes from the training set and return their associated sequences. This ensures that decoded sequences remain within the support of the observed data distribution.

Neural decoding. To enable sequence generation beyond the observed dataset, we introduce a latent-conditioned mutation decoder. Instead of generating sequences autoregressively, the decoder predicts mutation patterns relative to a wild-type sequence. For each position, the model predicts (i) whether a mutation occurs and (ii) the identity of the mutated amino acid. This formulation leverages the structure of deep mutational scanning datasets, where sequences differ from a common backbone.

Discussion. We find that decoding performance strongly depends on the structure of the latent space. In particular, PCA-based binary representations produce significantly more decodable latent codes than both random projections and AE/VAE representations. These results emphasize that representation learning must be aligned with both optimization and decoding objectives.

3.8 Quantum Annealing Compatibility

An important property of Q-BioLAT is that its optimization objective is already expressed in QUBO form. This means the learned latent fitness landscape can be optimized not only with classical combinatorial solvers, but also with quantum annealing hardware or other Ising/QUBO solvers without changing the model formulation. In this sense, Q-BioLAT provides a quantum-compatible interface between protein representation learning and discrete optimization.

In the present work, we focus on classical solvers to establish the feasibility of the framework and to analyze the optimization behavior in binary latent space. Nevertheless, the QUBO formulation opens a clear pathway toward future quantum-assisted protein engineering, where learned latent fitness landscapes could be deployed on quantum annealers or related specialized optimization hardware.

3.9 Computational Complexity

Let m denote the binary latent dimension. The QUBO surrogate uses $m + \frac{m(m-1)}{2} = O(m^2)$ features. Therefore, increasing latent dimensionality increases expressive power but also increases both the number of surrogate parameters and the difficulty of combinatorial search. This trade-off motivates our experimental study over multiple latent dimensions.

By separating the dense protein language model embedding stage from the binary optimization stage, Q-BioLAT keeps the most expensive neural computation fixed while enabling fast repeated optimization in the compact binary latent space. This makes the framework computationally attractive for studying representation-optimization trade-offs.

4 Experiments

Our experimental study is designed to answer three questions:

1. First, can an external sequence-level oracle trained from protein language model embeddings provide a reliable black-box fitness signal, especially in data-scarce settings?
2. Second, how do learned latent representations such as AE and VAE compare with simple projection-based binary codes for downstream optimization and decoding?
3. Third, does the full Q-BioLAT pipeline—from sequence embedding to latent optimization and decoding—produce

high-fitness candidate proteins under a fixed design budget?

Consistent with the scope of this work, we place the main emphasis on end-to-end protein design performance, while using the landscape analysis as a secondary interpretive layer.

4.1 Datasets and Data-Scarce Regimes

We evaluate Q-BioLAT on protein fitness landscapes from the ProteinGym benchmark [3]. Our primary experiments focus on two representative tasks: GFP and AAV. These two datasets provide complementary settings for studying both mutation-effect prediction and optimization over rugged protein fitness landscapes. For each dataset, we construct subset sizes of $\{1000, 2000, 5000, 10000\}$ variants (see Table 1). We treat the 1000 and 2000 settings as *data-scarce regimes*, and the 5000 and 10000 settings as *moderate-data regimes*. Unless otherwise specified, each subset is split into training, validation, and test sets using a stratified split based on fitness quantiles, with the validation split used for model selection and the test split reserved for final reporting. All reported results are averaged over multiple random seeds.

4.2 External Sequence-Level Fitness Oracle

A central component of this work is an external oracle that maps a protein sequence directly to a scalar fitness estimate. This oracle is conceptually distinct from the internal Q-BioLAT QUBO surrogate. The external oracle serves two purposes: (i) it provides a standardized black-box evaluator for comparing protein design methods that output sequences, and (ii) it enables evaluation of generated sequences that do not exactly match an experimentally observed variant.

For each protein sequence, we compute an ESM-based sequence embedding by mean pooling residue-level representations. On top of these embeddings, we train a family of classical regression models, including ridge regression, gradient-boosted decision trees (XGBoost), and Gaussian process regression. All models are trained on the same embedding space to isolate the effect of the regression model rather than the upstream representation. Model selection is performed using a validation split, and the best-performing oracle for each dataset-size regime is used in the downstream sequence-level optimization experiments.

We evaluate the external oracle using standard regression metrics, including Spearman correlation, Pearson correlation, root mean squared error (RMSE), and mean absolute error (MAE). Table 2 summarizes the results across both GFP and AAV datasets, and Figure 2 visualizes the scaling behavior.

Across both datasets, we observe a consistent and systematic dependence of oracle performance on the amount of available data. In both low-data regimes (1000–2000 samples) and moderate-data regimes (5000–10000 samples), Gaussian

Table 1. ProteinGym datasets used in the experiments. We consider two representative protein fitness landscapes: GFP for fluorescence-based fitness and AAV capsid for viral fitness. For each dataset, we construct multiple subset sizes to study data-scarce and moderate-data regimes.

Dataset	Task	WT length	Full library size	Subset sizes
GFP	Fluorescence / fitness	238	51,714	1000, 2000, 5000, 10000
AAV	Capsid / fitness	735	42,328	1000, 2000, 5000, 10000

process regression achieves the strongest performance, reflecting its ability to model uncertainty and adapt to limited supervision. As the dataset size increases, ridge regression becomes increasingly competitive and often achieves near the best performance, suggesting that the fitness signal is largely captured by a linear model in the ESM embedding space when sufficient data is available. In contrast, XGBoost underperforms in the smallest-data regime, indicating overfitting, but improves steadily with increasing dataset size. Based on these results, we use Gaussian process oracles in data-scarce settings when computationally feasible, and rely on ridge regression and XGBoost as scalable sequence-level evaluators in larger regimes.

4.3 Latent Representation Learning and Decoder Analysis

We compare four families of latent representations: (i) random projection with thresholding, (ii) PCA with thresholding, (iii) deterministic autoencoder (AE), and (iv) variational autoencoder (VAE). All methods operate on the same ESM embeddings to isolate the effect of latent representation.

Latent quality and collapse of learned representations.

We first examine whether learned latent models produce usable binary codes after binarization. Table 3 reports reconstruction error, bit entropy, and the number of active latent dimensions. Although AE and VAE achieve very low reconstruction error, their binarized latent codes exhibit near-zero entropy and essentially no active dimensions. This indicates a collapse of the binary latent space, where most bits become constant across samples and fail to encode meaningful variation. As a result, these representations do not provide a useful combinatorial search space for downstream optimization.

Decoding performance of projection-based representations. We next evaluate the decodability of binary latent codes using a mutation-conditioned decoder. Table 4 shows that projection-based representations, particularly PCA, significantly outperform random projections in both mutation F1 and mutated-residue accuracy. For example, on AAV with 10000 training samples, PCA with 64 latent dimensions achieves substantially higher decoding accuracy than random projection at the same dimensionality. Similar trends hold in the data-scarce regime on GFP.

Scaling behavior with data and latent dimension. Figure 3 further illustrates how decoding performance scales with the number of training samples at a fixed latent dimension of 64 bits. Across both GFP and AAV datasets, PCA consistently achieves higher mutation F1 than random projection, and performance improves as more data becomes available. This indicates that PCA not only preserves meaningful structure but also benefits from additional supervision.

Discussion. Taken together, these results reveal a clear mismatch between reconstruction quality and optimization readiness. While AE and VAE reconstruct embeddings accurately, their binarized latent spaces collapse and fail to support decoding or combinatorial search. In contrast, simple structured representations such as PCA maintain both variability and decodability, leading to substantially better downstream performance. These findings motivate our focus on PCA-based binary latent representations in the end-to-end design benchmark. These observations also suggest that latent representations for protein design should be evaluated not only by reconstruction or predictive accuracy, but by their ability to support both decoding and combinatorial optimization.

4.4 Internal QUBO Surrogate Performance

Given a binary latent representation, Q-BioLAT fits a quadratic surrogate over unary and pairwise latent features. This surrogate defines the QUBO objective used for combinatorial optimization. In this section, we evaluate how well different latent representations support the construction of such a surrogate.

Table 5 reports predictive performance of the learned QUBO models using Spearman correlation on held-out test data. Importantly, this evaluation is not intended to establish state-of-the-art fitness prediction, but rather to assess whether the latent representation induces a meaningful optimization landscape.

Across representations, we observe that PCA, random projection, and even AE/VAE can achieve comparable predictive performance under the QUBO surrogate. In particular, differences in Spearman correlation are often modest, indicating that multiple representations are capable of fitting observed fitness values to a similar degree.

However, when considered together with the results from Section 4.3 and the end-to-end benchmark in Section 4.6,

Table 2. Performance of external sequence-level fitness oracles built on top of ESM embeddings across GFP and AAV datasets. Results are reported on the test set. The best Spearman correlation for each dataset and training size is highlighted in bold.

Dataset	Train size	Oracle model	Spearman \uparrow	Pearson \uparrow	RMSE \downarrow	MAE \downarrow
GFP	1000	Gaussian Process	0.657	0.682	0.759	0.612
		Ridge Regression	0.637	0.665	0.859	0.652
		XGBoost	0.520	0.557	0.863	0.711
	2000	Gaussian Process	0.714	0.729	0.742	0.586
		Ridge Regression	0.660	0.669	0.817	0.637
		XGBoost	0.650	0.675	0.802	0.624
	5000	Gaussian Process	0.729	0.754	0.699	0.542
		Ridge Regression	0.702	0.697	0.772	0.607
		XGBoost	0.635	0.685	0.772	0.596
	10000	Gaussian Process	0.783	0.796	0.646	0.495
		Ridge Regression	0.735	0.730	0.730	0.580
		XGBoost	0.693	0.729	0.731	0.568
AAV	1000	Gaussian Process	0.671	0.650	2.390	1.906
		Ridge Regression	0.706	0.656	2.618	2.058
		XGBoost	0.611	0.607	2.501	2.005
	2000	Gaussian Process	0.792	0.762	2.048	1.629
		Ridge Regression	0.779	0.751	2.155	1.690
		XGBoost	0.694	0.694	2.255	1.813
	5000	Gaussian Process	0.806	0.782	1.898	1.505
		Ridge Regression	0.796	0.763	1.962	1.547
		XGBoost	0.729	0.724	2.094	1.659
	10000	Gaussian Process	0.838	0.821	1.712	1.346
		Ridge Regression	0.808	0.781	1.874	1.489
		XGBoost	0.777	0.772	1.914	1.499

Table 3. Collapse of learned latent representations after binarization on GFP with 1000 training samples. Although AE and VAE achieve low reconstruction error, their binarized latent codes exhibit zero entropy and no active dimensions.

Representation	Latent dim	Bit entropy \uparrow	Active dims \uparrow	Recon. MSE \downarrow
AE	8	0.000	0.00	0.000125
	64	0.000	0.00	0.000124
VAE	8	0.149	0.25	0.000126
	64	0.002	0.00	0.000164

a clear discrepancy emerges between predictive accuracy and optimization effectiveness. Although AE and VAE can achieve reasonable surrogate fits, their collapsed binary structure prevents effective decoding and downstream optimization. Similarly, random projection yields acceptable predictive performance but weaker decoding and design results compared to PCA.

These findings highlight a key distinction: predictive performance alone does not determine the usefulness of a representation for combinatorial optimization. Instead, the geometry of the latent space and its compatibility with decoding and search play a central role. This observation is consistent with the theoretical analysis in Section A, which shows that different representations can induce substantially different optimization landscapes even when predictive accuracy is similar.

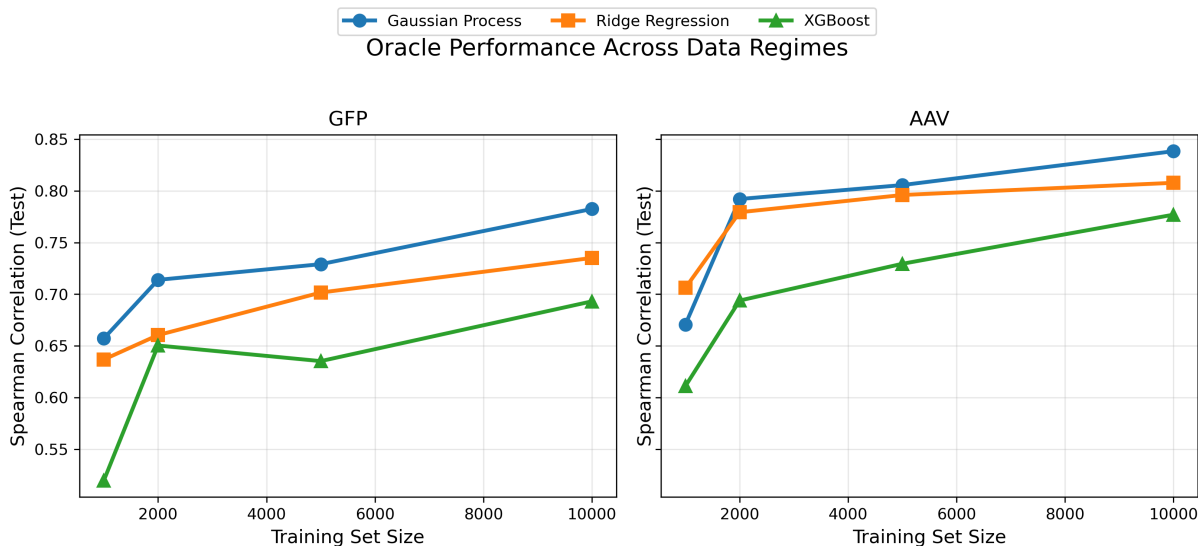


Figure 2. Test-set performance of external sequence-level fitness oracles across data regimes on GFP and AAV. Each panel shows the Spearman correlation between predicted and ground-truth fitness as a function of the number of training samples. Across both datasets, Gaussian process regression often achieves the strongest performance in both low-data and moderate-data regimes, reflecting its ability to model uncertainty under limited supervision. As the dataset size increases, ridge regression becomes increasingly competitive and often achieves near the best performance, indicating that the fitness signal is largely captured by a linear model in the ESM embedding space. In contrast, XGBoost underperforms in the smallest-data regime, suggesting overfitting, but improves steadily with additional data. These results establish a reliable sequence-level oracle for evaluating generated protein sequences and highlight the importance of selecting appropriate models under different data regimes.

Table 4. Decoding quality of projection-based binary latent representations. PCA consistently achieves higher mutation F1 and mutated-residue accuracy than random projection, and both metrics improve with increasing latent dimensionality. The better performance between two latent dimensions (i.e. bits) of 16 and 64 is highlighted in bold across different settings. The higher latent dimension (i.e. 64) consistently outperforms the lower latent dimension (i.e. 16) in decoding quality.

Dataset	Train size	Representation	Latent dim	Mutation F1 \uparrow	AA accuracy \uparrow
GFP	1000	PCA	16	0.110	0.551
		PCA	64	0.273	0.595
		Random	16	0.102	0.510
		Random	64	0.168	0.553
AAV	10000	PCA	16	0.369	0.367
		PCA	64	0.603	0.602
		Random	16	0.338	0.316
		Random	64	0.469	0.475

Overall, these results demonstrate that while the QUBO surrogate can be fitted across a range of representations, only structured latent spaces such as PCA lead to effective end-to-end protein design.

4.5 Conservative Retrieval-Based Optimization Benchmark

We evaluate Q-BioLAT in a conservative setting where optimized latent codes are mapped back to observed sequences via nearest-neighbor retrieval in Hamming space. This benchmark isolates the quality of the induced latent fitness landscape without confounding effects from neural decoding.

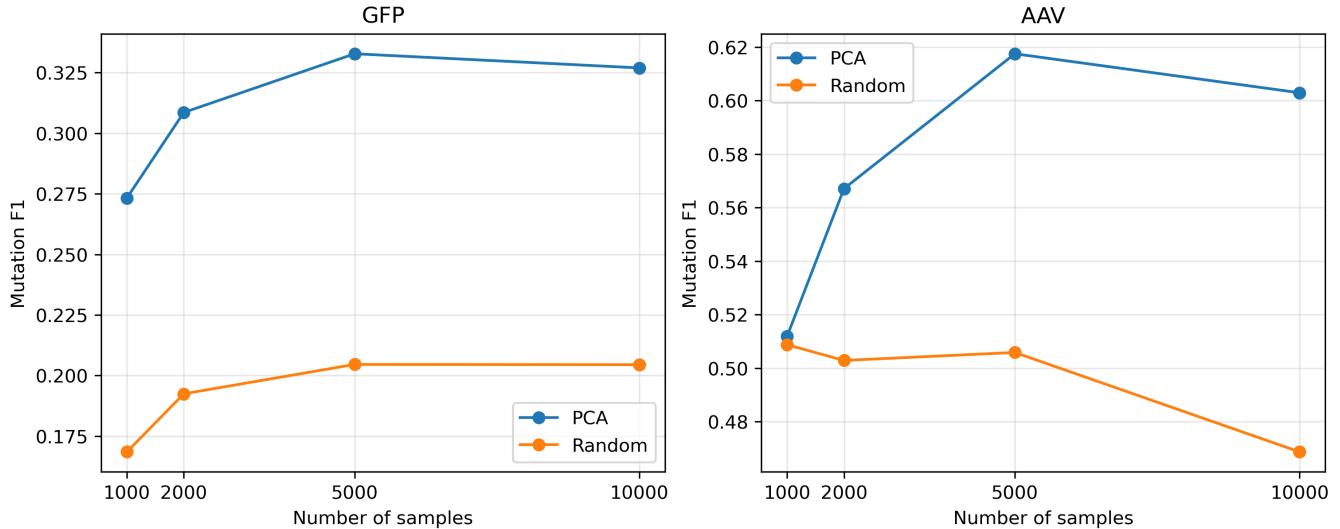


Figure 3. Scaling of decoding performance with dataset size for PCA-based and random-projection binary latent representations at 64 bits. The x-axis shows the number of training samples and the y-axis shows mutation F1. Across both GFP and AAV datasets, PCA consistently achieves higher decoding accuracy than random projection, and performance improves with increasing data.

Table 5. Predictive performance of the internal QUBO surrogate across latent representations, training data sizes, and latent dimensions. We report held-out test Spearman correlation. Although predictive differences are often modest, downstream optimization behavior differs substantially across representations. The better performance between the two binary-latent representations (i.e. PCA and random projection) is highlighted in bold. PCA outperforms random projection consistently in predictive quality of the internal QUBO surrogate across different settings.

Dataset	Train size	Latent dim	Representation	Spearman \uparrow
GFP	1000	16	Random	0.291
			PCA	0.147
	64	Random	0.196	
		PCA	0.277	
	10000	16	Random	0.302
			PCA	0.303
64	Random	0.413		
	PCA	0.532		
AAV	1000	16	Random	0.417
			PCA	0.393
	64	Random	0.407	
		PCA	0.511	
	10000	16	Random	0.366
			PCA	0.422
64	Random	0.534		
	PCA	0.564		

To ensure a fair comparison across optimization methods, all results are reported using PCA-based latent representations with a fixed latent dimension of 64 bits. Tables 6 and 7

summarize the mean retrieval-based optimization performance across multiseed runs on GFP and AAV, respectively.

Across both datasets and all data regimes, Simulated Annealing (SA), Genetic Algorithms (GA), and Greedy Hill Climb (GHC) consistently achieve strong performance, indicating that the induced QUBO landscape is well-structured for combinatorial search. In particular, these methods reliably identify high-fitness regions of the observed sequence manifold even in data-scarce settings, while latent Bayesian-style optimization (LBO) is generally less competitive.

These results demonstrate that PCA-based binary latent representations produce optimization-friendly landscapes that can be effectively explored by classical combinatorial solvers, providing a strong foundation for the full end-to-end design pipeline.

4.6 End-to-End Sequence Design Benchmark

We evaluate Q-BioLAT in an end-to-end protein design setting where optimized binary latent codes are decoded into protein sequences and scored using the external oracle. This benchmark directly measures whether optimization in binary latent space leads to improved sequence-level fitness.

Figure 4 summarizes the best end-to-end performance achieved by PCA-based and random-projection binary latent representations across training regimes on GFP and AAV. For each dataset and train size, we report the strongest configuration after jointly selecting the optimizer and latent dimension.

Across most settings, PCA-based binary latent representations achieve the strongest performance. This advantage is especially pronounced at moderate and larger data regimes, where higher-dimensional PCA latents (32 and 64 bits) consistently produce the highest oracle scores. These findings are consistent with the decoder analysis in Section 4.3, where PCA was shown to be substantially more decodable than both random projections and learned AE/VAE latent spaces.

We also observe that larger latent dimensions generally improve end-to-end performance, particularly for PCA, indicating that structured latent spaces can benefit from increased capacity without sacrificing decodability. In contrast, random projections are less reliable and usually underperform PCA, although a few low-data settings exhibit isolated exceptions.

Among the optimizers, Greedy Hill Climb (GHC), Genetic Algorithm (GA), and Simulated Annealing (SA) are consistently competitive, while latent Bayesian-style search (LBO) is generally weaker. Overall, these results show that Q-BioLAT provides an effective framework for end-to-end protein design, where binary latent optimization combined with structured representations enables the discovery of high-fitness protein sequences under a fixed oracle evaluation budget.

4.7 Data-Scarcity and Scaling Analysis

We next analyze how the performance of Q-BioLAT evolves as the amount of available fitness data increases. This experiment is particularly important because one of the primary motivations for using compact binary latent representations is to enable robust optimization under limited supervision.

Table 9 summarizes the best-performing oracle, latent representation, and design method across data regimes on both GFP and AAV. Several consistent patterns emerge.

Oracle behavior across data regimes. Across all datasets and training sizes, Gaussian process regression consistently provides the strongest sequence-level oracle. This highlights its ability to capture nonlinear structure in protein fitness landscapes and remain robust even as the dataset size increases. In contrast, simpler models such as ridge regression and XGBoost remain competitive but do not surpass Gaussian processes in our experiments.

Latent representation. Across all datasets and data regimes, PCA-based binary latent representations consistently provide the strongest performance. This observation aligns with the findings in Section 4.3, where PCA was shown to maintain high entropy, active latent dimensions, and strong decoding performance, while AE/VAE representations collapse after binarization.

Optimization methods. The best-performing design method varies with both dataset and data regime. In low-data settings, simpler methods such as Random Search (RS) and Greedy Hill Climbing (GHC) are often competitive, reflecting the relatively limited structure of the learned landscape. As the dataset size increases, more sophisticated combinatorial methods such as Genetic Algorithm (GA) and Simulated Annealing (SA) become increasingly effective, suggesting that the learned QUBO landscape becomes more informative and structured.

Scaling trends. We observe a clear transition from less stable behavior in the low-data regime (1000–2000 samples) to more consistent and high-performing optimization in the moderate-data regime (5000–10000 samples). In particular, PCA-based latent representations combined with higher latent dimensionality enable improved end-to-end performance, indicating that structured latent spaces can effectively leverage additional data without sacrificing decodability or optimization stability.

Summary. Overall, these results demonstrate that Q-BioLAT provides a robust framework for protein design across data regimes. The combination of a strong Gaussian process oracle, structured PCA-based latent representations, and combinatorial optimization enables effective identification of high-fitness sequences, particularly in data-scarce settings, while continuing to improve as more data becomes available.

Table 6. Retrieval-based optimization results on GFP using PCA latent representations with 64 bits. Each row reports the mean performance across multiseed runs for one optimizer. Optimizers include Simulated Annealing (SA), Genetic Algorithm (GA), Random Search (RS), Greedy Hill Climb (GHC), and Latent Bayesian Optimization (LBO). In each data size, the best performance in each metric is highlighted in bold.

Train size	Optimizer	Improvement \uparrow	NN fitness \uparrow	Percentile \uparrow
1000	SA	4.978	3.568	73.200
	GA	5.044	3.440	60.925
	RS	1.750	3.443	58.650
	GHC	4.918	3.616	74.825
	LBO	-1.509	2.766	58.050
2000	SA	11.529	3.558	70.700
	GA	11.103	2.908	62.025
	RS	4.770	2.593	43.175
	GHC	10.230	3.580	75.013
	LBO	-1.119	2.953	47.700
5000	SA	6.757	3.479	63.410
	GA	6.628	3.689	83.330
	RS	2.617	3.078	61.640
	GHC	6.083	3.761	80.605
	LBO	-1.005	2.775	54.085
10000	SA	4.162	3.220	69.740
	GA	3.938	3.607	74.595
	RS	1.609	3.590	71.938
	GHC	3.688	3.175	64.562
	LBO	-1.253	1.836	28.780

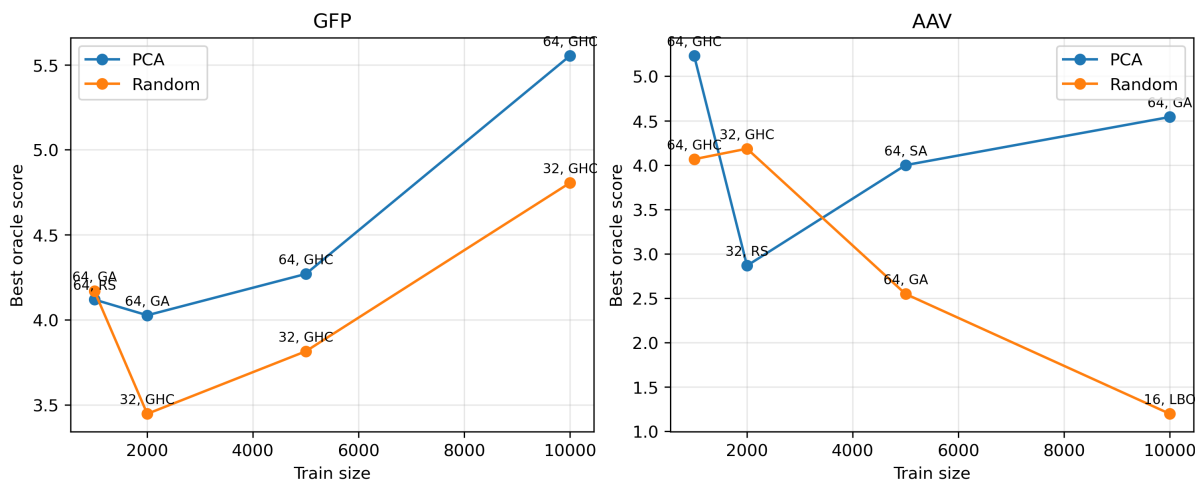


Figure 4. End-to-end sequence design performance after optimization, decoding, and oracle scoring. For each dataset and training size, we plot the best-performing PCA-based and random-projection configuration. Each point is annotated with the corresponding latent dimension and optimizer. Across most settings, PCA-based binary latent representations achieve the strongest sequence-level performance, particularly at moderate and larger data regimes.

4.8 Implementation Details and Reporting Protocol

Unless otherwise specified, all methods use the same upstream ESM embedding extractor in order to isolate the effect

Table 7. Retrieval-based optimization results on AAV using PCA latent representations with 64 bits. Each row reports the mean performance across multiseed runs for one optimizer. Optimizers include Simulated Annealing (SA), Genetic Algorithm (GA), Random Search (RS), Greedy Hill Climb (GHC), and Latent Bayesian Optimization (LBO). In each data size, the best performance in each metric is highlighted in bold.

Train size	Optimizer	Improvement \uparrow	NN fitness \uparrow	Percentile \uparrow
1000	SA	11.364	3.303	88.225
	GA	10.342	3.949	90.000
	RS	1.224	1.945	77.550
	GHC	9.362	3.902	91.400
	LBO	-9.071	-0.606	53.200
2000	SA	28.756	1.794	72.275
	GA	27.108	-1.256	47.325
	RS	8.523	0.343	66.050
	GHC	26.511	1.856	74.388
	LBO	-11.177	-0.116	61.725
5000	SA	14.627	-0.654	50.165
	GA	13.636	3.869	95.325
	RS	4.153	1.477	77.715
	GHC	13.162	6.643	94.975
	LBO	-5.378	-1.871	44.250
10000	SA	12.575	3.038	86.198
	GA	12.321	3.720	92.948
	RS	4.115	2.278	78.420
	GHC	11.545	3.262	91.380
	LBO	-3.503	0.003	61.045

of latent representation and optimization strategy. Hyperparameters are selected on the validation split, and final results are reported on the held-out test split or on oracle-evaluated generated candidates, depending on the experiment. For design methods, we use a fixed candidate budget and report both the best returned sequence and the average performance of the top- K returned candidates. All reported means and standard deviations are computed over multiple random seeds. For this work, we publicly release code, exact hyperparameter settings, and scripts for reproducing all tables and figures at:

<https://github.com/HySonLab/Q-BIOLAT-Extended>

5 Conclusion

In this work, we introduced Q-BioLAT, a framework for modeling and optimizing protein fitness landscapes in compact binary latent spaces. By transforming protein sequence representations into binary codes and learning a quadratic unconstrained binary optimization (QUBO) surrogate, Q-BioLAT enables direct application of combinatorial optimization methods to protein design.

Beyond its algorithmic formulation, our central contribution is a representation-centric perspective on protein fitness modeling. We show both theoretically and empirically that

predictive accuracy alone is insufficient for effective optimization. Instead, the geometry of the latent space—captured through its induced QUBO interactions—plays a decisive role in determining search behavior, landscape smoothness, and the ability to identify high-fitness sequences.

Our experiments demonstrate three key findings. First, learned autoencoder-based representations collapse under binarization and fail to support optimization, despite achieving low reconstruction error. Second, simple structured representations such as PCA consistently produce more informative and decodable latent spaces, leading to better optimization performance. Third, combinatorial optimization methods such as simulated annealing, genetic algorithms, and greedy hill climbing are highly effective when applied to these structured binary latent landscapes, especially when combined with a strong sequence-level oracle.

We further show that Q-BioLAT performs robustly across data regimes, including data-scarce settings where traditional methods often struggle. As more data becomes available, both oracle quality and latent structure improve, leading to increasingly effective end-to-end protein design.

Table 8. End-to-end protein design benchmark under a fixed external-oracle evaluation budget. For each dataset and train size, we report the best-performing random-projection and PCA-based Q-BioLAT configuration after optimization, decoding, and oracle scoring. Optimizers include Simulated Annealing (SA), Genetic Algorithm (GA), Random Search (RS), Greedy Hill Climb (GHC), and Latent Bayesian Optimization (LBO). The better performance between PCA and random projection is highlighted in bold.

Dataset	Train size	Representation	Optimizer	Latent dim	Best score \uparrow	Top-10 mean \uparrow
GFP	1000	PCA	RS	64	4.119	3.903
		Random	GA	64	4.170	3.312
	2000	PCA	GA	64	4.027	3.549
		Random	GHC	32	3.448	2.693
	5000	PCA	GHC	64	4.270	3.972
		Random	GHC	32	3.815	2.228
10000	PCA	GHC	64	5.554	5.042	
	Random	GHC	32	4.806	3.829	
AAV	1000	PCA	GHC	64	5.232	2.962
		Random	GHC	64	4.066	-1.557
	2000	PCA	RS	32	2.866	0.349
		Random	GHC	32	4.184	-2.674
	5000	PCA	SA	64	3.999	2.249
		Random	GA	64	2.548	-1.150
	10000	PCA	GA	64	4.541	2.091
		Random	LBO	16	1.197	-4.205

Table 9. Scaling summary across data regimes. We report the best-performing oracle, latent representation, and design method as a function of available training data.

Dataset	Train size	Best oracle	Best latent representation	Best design method
GFP	1000	Gaussian Process	PCA	Random Search (RS)
	2000	Gaussian Process	PCA	Genetic Algorithm (GA)
	5000	Gaussian Process	PCA	Greedy Hill Climb (GHC)
	10000	Gaussian Process	PCA	Greedy Hill Climb (GHC)
AAV	1000	Gaussian Process	PCA	Greedy Hill Climb (GHC)
	2000	Gaussian Process	PCA	Random Search (RS)
	5000	Gaussian Process	PCA	Simulated Annealing (SA)
	10000	Gaussian Process	PCA	Genetic Algorithm (GA)

Overall, Q-BioLAT bridges protein language modeling, discrete representation learning, and combinatorial optimization, providing a principled framework for optimization-aware protein fitness modeling. By explicitly modeling the latent fitness landscape as a QUBO problem, our approach naturally connects modern machine learning with classical and quantum optimization paradigms. This opens several promising directions for future work, including integration with quantum annealing hardware, development of optimization-aware representation learning methods, and extension to multi-objective and constrained protein design.

References

- [1] Philip A Romero and Frances H Arnold. Exploring protein fitness landscapes by directed evolution. *Nature reviews Molecular cell biology*, 10(12):866–876, 2009.
- [2] Lin Chen, Zehong Zhang, Zhenghao Li, Rui Li, Ruifeng Huo, Lifan Chen, Dingyan Wang, Xiaomin Luo, Kaixian Chen, Cangsong Liao, and Mingyue Zheng. Learning protein fitness landscapes with deep mutational scanning data from multiple sources. *Cell Systems*, 14(8):706–721.e5, 2023. ISSN 2405-4712. doi: <https://doi.org/10.1016/j.cels.2023.07.003>. URL <https://www.sciencedirect.com/science/article/pii/S2405471223002107>.
- [3] Pascal Notin, Aaron Kollasch, Daniel Ritter, Lood van Niekerk, Stefanie Paul, Han Spinner, Nathan Rollins, Ada Shaw, Rose Orenbuch,

- Ruben Weitzman, Jonathan Frazer, Mafalda Dias, Dinko Franceschi, Yarin Gal, and Debora Marks. Proteingym: Large-scale benchmarks for protein fitness prediction and design. In A. Oh, T. Naumann, A. Globerson, K. Saenko, M. Hardt, and S. Levine, editors, *Advances in Neural Information Processing Systems*, volume 36, pages 64331–64379. Curran Associates, Inc., 2023. URL https://proceedings.neurips.cc/paper_files/paper/2023/file/cac723e5ff29f65e3fcb0739ae91bee-Paper-Datasets_and_Benchmarks.pdf.
- [4] Zeming Lin, Halil Akin, Roshan Rao, Brian Hie, Zhongkai Zhu, Wenting Lu, Nikita Smetanin, Robert Verkuil, Ori Kabeli, Yaniv Shmueli, Allan dos Santos Costa, Maryam Fazel-Zarandi, Tom Sercu, Salvatore Candido, and Alexander Rives. Evolutionary-scale prediction of atomic-level protein structure with a language model. *Science*, 379(6637):1123–1130, 2023. doi: 10.1126/science.ade2574. URL <https://www.science.org/doi/abs/10.1126/science.ade2574>.
 - [5] Thomas Hayes, Roshan Rao, Halil Akin, Nicholas J. Sofroniew, Deniz Oktay, Zeming Lin, Robert Verkuil, Vincent Q. Tran, Jonathan Deaton, Marius Wiggert, Rohil Badkundri, Irhum Shafkat, Jun Gong, Alexander Derry, Raul S. Molina, Neil Thomas, Yousuf A. Khan, Chetan Mishra, Carolyn Kim, Liam J. Bartie, Matthew Nemeth, Patrick D. Hsu, Tom Sercu, Salvatore Candido, and Alexander Rives. Simulating 500 million years of evolution with a language model. *Science*, 387(6736):850–858, 2025. doi: 10.1126/science.ads0018. URL <https://www.science.org/doi/abs/10.1126/science.ads0018>.
 - [6] Céline Marquet, Julius Schlenzok, Marina Abakarova, Burkhard Rost, and Elodie Laine. Expert-guided protein language models enable accurate and blazingly fast fitness prediction. *Bioinformatics*, 40(11):btac621, 11 2024. ISSN 1367-4811. doi: 10.1093/bioinformatics/btac621. URL <https://doi.org/10.1093/bioinformatics/btac621>.
 - [7] Dan Liu, Francesca Young, Kieran D Lamb, Adalberto Claudio Quiros, Alexandrina Pancheva, Crispin J Miller, Craig Macdonald, David L Robertson, and Ke Yuan. Plm-interact: extending protein language models to predict protein-protein interactions. *Nature Communications*, 16(1):9012, 2025.
 - [8] Joseph L Watson, David Juergens, Nathaniel R Bennett, Brian L Trippe, Jason Yim, Helen E Eisenach, Woody Ahern, Andrew J Borst, Robert J Ragotte, Lukas F Milles, et al. De novo design of protein structure and function with rfdiffusion. *Nature*, 620(7976):1089–1100, 2023.
 - [9] Thanh V T Tran, Nhat Khang Ngo, Viet Thanh Duy Nguyen, and Truong-Son Hy. Latentde: latent-based directed evolution for protein sequence design. *Machine Learning: Science and Technology*, 6(1):015070, mar 2025. doi: 10.1088/2632-2153/adc2e2. URL <https://doi.org/10.1088/2632-2153/adc2e2>.
 - [10] Thanh V. T. Tran and Truong Son Hy. Protein design by directed evolution guided by large language models. *IEEE Transactions on Evolutionary Computation*, 29(2):418–428, 2025. doi: 10.1109/TEVC.2024.3439690.
 - [11] Hiroki Ozawa, Ibuki Unno, Ryohei Sekine, Taichi Chisuga, Sohei Ito, and Shogo Nakano. Development of evolutionary algorithm-based protein redesign method. *Cell Reports Physical Science*, 5(1):101758, 2024. ISSN 2666-3864. doi: <https://doi.org/10.1016/j.xcrp.2023.101758>. URL <https://www.sciencedirect.com/science/article/pii/S2666386423006033>.
 - [12] Timothy Atkinson, Thomas D Barrett, Scott Cameron, Bora Guloglu, Matthew Greenig, Charlie B Tan, Louis Robinson, Alex Graves, Liviu Copoiu, and Alexandre Laterre. Protein sequence modelling with bayesian flow networks. *Nature Communications*, 16(1):3197, 2025.
 - [13] Ruyun Hu, Lihao Fu, Yongcan Chen, Junyu Chen, Yu Qiao, and Tong Si. Protein engineering via bayesian optimization-guided evolutionary algorithm and robotic experiments. *Briefings in Bioinformatics*, 24(1):bbac570, 12 2022. ISSN 1477-4054. doi: 10.1093/bib/bbac570. URL <https://doi.org/10.1093/bib/bbac570>.
 - [14] Gary Kochenberger, Jin-Kao Hao, Fred Glover, Mark Lewis, Zhipeng Lü, Haibo Wang, and Yang Wang. The unconstrained binary quadratic programming problem: a survey. *Journal of combinatorial optimization*, 28(1):58–81, 2014.
 - [15] Andrew Lucas. Ising formulations of many np problems. *Frontiers in Physics*, Volume 2 - 2014, 2014. ISSN 2296-424X. doi: 10.3389/fphy.2014.00005. URL <https://www.frontiersin.org/journals/physics/articles/10.3389/fphy.2014.00005>.
 - [16] Seongmin Kim, Sang-Woo Ahn, In-Saeng Suh, Alexander W Dowling, Eungkyu Lee, and Tengfei Luo. Quantum annealing for combinatorial optimization: a benchmarking study. *npj Quantum Information*, 11(1):77, 2025.
 - [17] Viet Thanh Duy Nguyen and Truong Son Hy. Multimodal pretraining for unsupervised protein representation learning. *Biology Methods and Protocols*, 9(1):bpae043, 06 2024. ISSN 2396-8923. doi: 10.1093/biomethods/bpae043. URL <https://doi.org/10.1093/biomethods/bpae043>.
 - [18] Nhat Khang Ngo and Truong Son Hy. Multimodal protein representation learning and target-aware variational auto-encoders for protein-binding ligand generation. *Machine Learning: Science and Technology*, 5(2):025021, apr 2024. doi: 10.1088/2632-2153/ad3ee4. URL <https://doi.org/10.1088/2632-2153/ad3ee4>.
 - [19] Alexander Rives, Joshua Meier, Tom Sercu, Siddharth Goyal, Zeming Lin, Jason Liu, Demi Guo, Myle Ott, C. Lawrence Zitnick, Jerry Ma, and Rob Fergus. Biological structure and function emerge from scaling unsupervised learning to 250 million protein sequences. *Proceedings of the National Academy of Sciences*, 118(15):e2016239118, 2021. doi: 10.1073/pnas.2016239118. URL <https://www.pnas.org/doi/abs/10.1073/pnas.2016239118>.
 - [20] Zeming Lin, Halil Akin, Roshan Rao, Brian Hie, Zhongkai Zhu, Wenting Lu, Nikita Smetanin, Robert Verkuil, Ori Kabeli, Yaniv Shmueli, et al. Evolutionary-scale prediction of atomic-level protein structure with a language model. *Science*, 379(6637):1123–1130, 2023.
 - [21] Kevin K Yang, Zachary Wu, and Frances H Arnold. Machine-learning-guided directed evolution for protein engineering. *Nature methods*, 16(8):687–694, 2019.
 - [22] Surojit Biswas, Grigory Khimulya, Ethan C Alley, Kevin M Esvelt, and George M Church. Low-n protein engineering with data-efficient deep learning. *Nature methods*, 18(4):389–396, 2021.
 - [23] Fanhao Wang, Tiantian Zhang, Jintao Zhu, Xiaoling Zhang, Changsheng Zhang, and Luhua Lai. Reinforcement learning-based target-specific de novo design of cyclic peptide binders. *Journal of Medicinal Chemistry*, 68(16):17287–17302, 2025.
 - [24] Haoran Sun, Liang He, Pan Deng, Guoqing Liu, Zhiyu Zhao, Yuliang Jiang, Chuan Cao, Fusong Ju, Lijun Wu, Haiguang Liu, et al. Accelerating protein engineering with fitness landscape modelling and reinforcement learning. *Nature Machine Intelligence*, 7(9):1446–1460, 2025.
 - [25] Optimization by simulated annealing. *science*, 220(4598):671–680, 1983.
 - [26] John H. Holland. *Adaptation in Natural and Artificial Systems: An Introductory Analysis with Applications to Biology, Control, and Artificial Intelligence*. The MIT Press, 04 1992. ISBN 9780262275552. doi: 10.7551/mitpress/1090.001.0001. URL <https://doi.org/10.7551/mitpress/1090.001.0001>.
 - [27] Mark W. Johnson, Mohammad H. S. Amin, Gildert Suzanne, Trevor Lanting, Firas Hamze, Neil G. Dickson, Richard G. Harris, Andrew J. Berkley, J. Johansson, Paul I. Bunyk, E. M. Chapple, Colin Enderud, Jeremy P. Hilton, Kamran Karimi, Eric Ladizinsky, Nicolas Ladizinsky, Travis Oh, I. G. Perminov, Chris Rich, Murray C. Thom, Elena Tolka-cheva, C. J. S. Truncik, Sergey Uchaikin, J. Wang, Blake A. Wilson, and Georgie Rose. Quantum annealing with manufactured spins. *Nature*, 473:194–198, 2011. URL <https://api.semanticscholar.org/CorpusID:205224761>.
 - [28] André Hottung, Bhanu Bhandari, and Kevin Tierney. Learning a latent search space for routing problems using variational autoencoders. In *International Conference on Learning Representations*, 2021. URL

- <https://openreview.net/forum?id=90JprVrJBO>.
- [29] Peter J. Bentley, Soo Ling Lim, Adam Gaier, and Linh Tran. Coil: Constrained optimization in learned latent space: learning representations for valid solutions. In *Proceedings of the Genetic and Evolutionary Computation Conference Companion*, GECCO '22, page 1870–1877, New York, NY, USA, 2022. Association for Computing Machinery. ISBN 9781450392686. doi: 10.1145/3520304.3533993. URL <https://doi.org/10.1145/3520304.3533993>.
- [30] Dhruv Menon and Raghavan Ranganathan. A generative approach to materials discovery, design, and optimization. *ACS Omega*, 7(30): 25958–25973, 2022. doi: 10.1021/acsomega.2c03264. URL <https://doi.org/10.1021/acsomega.2c03264>.
- [31] Truong Son Hy and Risi Kondor. Multiresolution equivariant graph variational autoencoder. *Machine Learning: Science and Technology*, 4(1):015031, mar 2023. doi: 10.1088/2632-2153/acc0d8. URL <https://doi.org/10.1088/2632-2153/acc0d8>.
- [32] Mingrui Jiang, Keyi Shan, Chengping He, and Can Li. Efficient combinatorial optimization by quantum-inspired parallel annealing in analogue memristor crossbar. *Nature Communications*, 14(1):5927, 2023.
- [33] Tetsuro Abe, Masashi Yamashita, and Shu Tanaka. Effectiveness of binary autoencoders for qubo-based optimization problems. *arXiv preprint arXiv:2602.10037*, 2026.
- [34] Marc Mézard and Andrea Montanari. *Information, Physics, and Computation*. Oxford University Press, 01 2009. ISBN 9780198570837. doi: 10.1093/acprof:oso/9780198570837.001.0001. URL <https://doi.org/10.1093/acprof:oso/9780198570837.001.0001>.
- [35] David Wales. *Energy Landscapes: Applications to Clusters, Biomolecules and Glasses*. Cambridge Molecular Science. Cambridge University Press, 2004.
- [36] Antonio Auffinger, Gérard Ben Arous, and Jiří Černý. Random matrices and complexity of spin glasses. *Communications on Pure and Applied Mathematics*, 66(2):165–201, 2013. doi: <https://doi.org/10.1002/cpa.21422>. URL <https://onlinelibrary.wiley.com/doi/abs/10.1002/cpa.21422>.
- [37] Anna Choromanska, Mlkael Henaff, Michael Mathieu, Gerard Ben Arous, and Yann LeCun. The Loss Surfaces of Multilayer Networks. In Guy Lebanon and S. V. N. Vishwanathan, editors, *Proceedings of the Eighteenth International Conference on Artificial Intelligence and Statistics*, volume 38 of *Proceedings of Machine Learning Research*, pages 192–204, San Diego, California, USA, 09–12 May 2015. PMLR. URL <https://proceedings.mlr.press/v38/choromanska15.html>.
- [38] Ian Goodfellow, Oriol Vinyals, and Andrew Saxe. Qualitatively characterizing neural network optimization problems. In *International Conference on Learning Representations*, 2015. URL <http://arxiv.org/abs/1412.6544>.
- [39] Rafael Gómez-Bombarelli, Jennifer N. Wei, David Duvenaud, José Miguel Hernández-Lobato, Benjamín Sánchez-Lengeling, Dennis Sheberla, Jorge Aguilera-Iparraguirre, Timothy D. Hirzel, Ryan P. Adams, and Alán Aspuru-Guzik. Automatic chemical design using a data-driven continuous representation of molecules. *ACS Central Science*, 4(2):268–276, 2018. doi: 10.1021/acscentsci.7b00572. URL <https://doi.org/10.1021/acscentsci.7b00572>. PMID: 29532027.
- [40] Wengong Jin, Regina Barzilay, and Tommi Jaakkola. Junction tree variational autoencoder for molecular graph generation. In Jennifer Dy and Andreas Krause, editors, *Proceedings of the 35th International Conference on Machine Learning*, volume 80 of *Proceedings of Machine Learning Research*, pages 2323–2332. PMLR, 10–15 Jul 2018. URL <https://proceedings.mlr.press/v80/jin18a.html>.
- [41] Ryan-Rhys Griffiths and José Miguel Hernández-Lobato. Constrained bayesian optimization for automatic chemical design using variational autoencoders. *Chem. Sci.*, 11:577–586, 2020. doi: 10.1039/C9SC04026A. URL <http://dx.doi.org/10.1039/C9SC04026A>.
- [42] ANM Nafiz Abeer, Nathan M Urban, M Ryan Weil, Francis J Alexander, and Byung-Jun Yoon. Multi-objective latent space optimization of generative molecular design models. *Patterns*, 5(10), 2024.
- [43] Yoshua Bengio, Aaron Courville, and Pascal Vincent. Representation learning: A review and new perspectives. *IEEE Trans. Pattern Anal. Mach. Intell.*, 35(8):1798–1828, August 2013. ISSN 0162-8828. doi: 10.1109/TPAMI.2013.50. URL <https://doi.org/10.1109/TPAMI.2013.50>.
- [44] Piotr Bojanowski, Armand Joulin, David Lopez-Pas, and Arthur Szlam. Optimizing the latent space of generative networks. In Jennifer Dy and Andreas Krause, editors, *Proceedings of the 35th International Conference on Machine Learning*, volume 80 of *Proceedings of Machine Learning Research*, pages 600–609. PMLR, 10–15 Jul 2018. URL <https://proceedings.mlr.press/v80/bojanowski18a.html>.
- [45] G. E. Hinton and R. R. Salakhutdinov. Reducing the dimensionality of data with neural networks. *Science*, 313(5786):504–507, 2006. doi: 10.1126/science.1127647. URL <https://www.science.org/doi/abs/10.1126/science.1127647>.
- [46] Pascal Vincent, Hugo Larochelle, Isabelle Lajoie, Yoshua Bengio, and Pierre-Antoine Manzagol. Stacked denoising autoencoders: Learning useful representations in a deep network with a local denoising criterion. *J. Mach. Learn. Res.*, 11:3371–3408, December 2010. ISSN 1532-4435.
- [47] Diederik P Kingma and Max Welling. Auto-encoding variational bayes. *arXiv preprint arXiv:1312.6114*, 2013.

A Theoretical Insights into Binary Latent Fitness Landscapes

In this section, we provide a theoretical perspective on how binary latent representations induce structured optimization landscapes, and how their geometry affects combinatorial search.

A.1 QUBO as an Energy Landscape

Recall that the QUBO surrogate defines the predicted fitness of a binary latent code $x \in \{0, 1\}^m$ as:

$$\hat{f}(x) = h^\top x + \frac{1}{2} x^\top J x, \quad (9)$$

where $h \in \mathbb{R}^m$ and $J \in \mathbb{R}^{m \times m}$ is a symmetric interaction matrix. This formulation can be equivalently interpreted as an energy-based model:

$$E(x) = -\hat{f}(x), \quad (10)$$

where optimization corresponds to finding low-energy configurations.

Under this view, the binary latent space $\{0, 1\}^m$ forms a discrete configuration space (a Boolean hypercube), and the QUBO defines an energy landscape over its vertices. The structure of this landscape is fully determined by the parameters (h, J) , which in turn depend on the choice of latent representation.

A.2 Local Geometry and Bit-Flip Dynamics

A fundamental operation in combinatorial optimization is a single-bit flip. Let $x^{(k)}$ denote the vector obtained by flipping the k -th bit of x . The change in predicted fitness is:

$$\Delta_k(x) = \hat{f}(x^{(k)}) - \hat{f}(x). \quad (11)$$

For the QUBO model, this quantity can be expressed explicitly as:

$$\Delta_k(x) = (1 - 2x_k) \left(h_k + \sum_{\ell \neq k} J_{k\ell} x_\ell \right). \quad (12)$$

This expression shows that local search behavior is governed by the interaction structure of J . In particular:

- The term h_k captures the intrinsic contribution of the k -th latent dimension.
- The sum $\sum_{\ell} J_{k\ell} x_\ell$ captures how other latent variables influence the effect of flipping bit k .

Thus, optimization trajectories depend not only on the current state x , but also on the global interaction structure encoded in J .

A.3 Landscape Smoothness and Ruggedness

The difficulty of optimization is closely related to the smoothness of the energy landscape. We characterize local variability using the variance of $\Delta_k(x)$ over the latent space:

$$\text{Var}[\Delta_k(x)] \approx \sum_{\ell} J_{k\ell}^2. \quad (13)$$

This suggests that the norm of the interaction coefficients controls the ruggedness of the landscape:

- Small $\|J_k\|$ leads to smoother landscapes with more predictable local improvements.
- Large $\|J_k\|$ leads to highly variable local changes and a proliferation of local optima.

Consequently, the structure of J plays a central role in determining optimization difficulty.

A.4 Spectral Structure of the Interaction Matrix

Further insight can be obtained by analyzing the spectrum of the interaction matrix J . Let $\{\lambda_i\}$ denote its eigenvalues. Then:

- Low-rank or structured J (few dominant eigenvalues) corresponds to landscapes with coherent global directions, facilitating optimization.
- Random or full-rank J with dispersed eigenvalues corresponds to more irregular, spin-glass-like landscapes with many local minima.

Since J is learned from latent representations, its spectral properties are directly influenced by the choice of representation (e.g., PCA vs random projection vs learned encoders).

A.5 Representation–Optimization Decoupling

A key implication of this analysis is that predictive performance alone does not determine optimization behavior. Two representations may yield similar surrogate accuracy (e.g., similar Spearman correlation), yet induce different interaction matrices J with distinct geometric properties.

Observation: Representations with similar predictive accuracy can induce fundamentally different optimization landscapes.

This phenomenon arises because predictive metrics evaluate pointwise accuracy, whereas optimization depends on the global structure of the energy landscape. As a result, representation learning for protein design should account not only for prediction quality, but also for the induced landscape geometry.

A.6 Implications for Latent Representation Design

The above analysis suggests several principles for designing effective latent representations:

- Structured representations (e.g., PCA or learned encoders) tend to produce smoother and more optimization-friendly landscapes.

- Overly high-dimensional latent spaces can increase model expressivity but also introduce ruggedness, making optimization more difficult.
- Learned representations can potentially balance expressivity and smoothness by aligning latent dimensions with fitness-relevant directions.

These insights provide a theoretical foundation for understanding the empirical observations in Section 4 and motivate the development of optimization-aware representation learning methods.

Here, we formalize how the learned binary representation determines the geometry, smoothness, and identifiability of the induced QUBO landscape. Our goal is not to solve the global QUBO exactly, but to characterize the quantities that govern local search, global variation, and the stability of the learned surrogate.

A.7 Energy Landscape and Local Fields

Recall that the QUBO surrogate defines the predicted fitness of a binary latent code $x \in \{0, 1\}^m$ as:

$$\hat{f}(x) = h^\top x + \frac{1}{2} x^\top J x, \quad (14)$$

where $h \in \mathbb{R}^m$ and $J \in \mathbb{R}^{m \times m}$ is a symmetric interaction matrix with zero diagonal. Equivalently, we may define the energy:

$$E(x) = -\hat{f}(x), \quad (15)$$

so that maximizing predicted fitness is equivalent to minimizing energy over the Boolean hypercube.

A useful quantity for analyzing this landscape is the *local field*:

$$g_k(x) = h_k + \sum_{\ell \neq k} J_{k\ell} x_\ell, \quad (16)$$

which measures the effective force acting on the k -th bit given the remaining coordinates.

Proposition (Bit-flip gain and local optimality). Let $x^{(k)}$ denote the binary code obtained by flipping the k -th bit of x . Then the change in predicted fitness induced by a single-bit flip is:

$$\Delta_k(x) = \hat{f}(x^{(k)}) - \hat{f}(x) = (1 - 2x_k) g_k(x). \quad (17)$$

Consequently, a binary code x^* is a local maximizer with respect to single-bit flips if and only if:

$$\Delta_k(x^*) \leq 0 \quad \text{for all } k, \quad (18)$$

or equivalently,

$$x_k^* = \begin{cases} 1, & g_k(x^*) \geq 0, \\ 0, & g_k(x^*) \leq 0, \end{cases} \quad (19)$$

with either value allowed when $g_k(x^*) = 0$.

Proof. Write $x^{(k)} = x + (1 - 2x_k)e_k$, where e_k is the k -th standard basis vector. Substituting into the QUBO objective and using the symmetry of J together with $J_{kk} = 0$ gives:

$$\hat{f}(x^{(k)}) - \hat{f}(x) = (1 - 2x_k) \left(h_k + \sum_{\ell \neq k} J_{k\ell} x_\ell \right).$$

The local-optimality condition follows immediately by requiring that no single-bit flip improves the objective. \square

This proposition shows that local search in Q-BioLAT is governed by the collection of local fields $\{g_k(x)\}_{k=1}^m$. In particular, the interaction matrix J determines how strongly each latent dimension depends on the current configuration of the others.

A.8 Hamming Smoothness and Spectral Control

We next quantify how much the QUBO objective can change between two latent codes.

Proposition (Hamming-Lipschitz continuity). For any $x, y \in \{0, 1\}^m$,

$$|\hat{f}(x) - \hat{f}(y)| \leq (\|h\|_\infty + \|J\|_\infty) d_H(x, y), \quad (20)$$

where $d_H(x, y)$ is the Hamming distance and $\|J\|_\infty = \max_k \sum_{\ell=1}^m |J_{k\ell}|$ is the matrix infinity norm.

Proof. Let $\delta = x - y$. Then $\|\delta\|_1 = d_H(x, y)$ and

$$\hat{f}(x) - \hat{f}(y) = h^\top \delta + \frac{1}{2} \delta^\top J (x + y). \quad (21)$$

Therefore,

$$|\hat{f}(x) - \hat{f}(y)| \leq \|h\|_\infty \|\delta\|_1 + \frac{1}{2} \|\delta\|_1 \|J\|_\infty \|x + y\|_\infty.$$

Since $x, y \in \{0, 1\}^m$, we have $\|x + y\|_\infty \leq 2$, which yields the result. \square

This result shows that the quantity

$$L_H := \|h\|_\infty + \|J\|_\infty \quad (22)$$

acts as a global smoothness constant of the landscape in Hamming space.

Corollary (Spectral control of landscape variation).

For any $x, y \in \{0, 1\}^m$,

$$|\hat{f}(x) - \hat{f}(y)| \leq \sqrt{d_H(x, y)} \left(\|h\|_2 + \sqrt{m} \|J\|_2 \right), \quad (23)$$

where $\|J\|_2$ denotes the spectral norm of J .

Proof. Using the same decomposition with $\delta = x - y$,

$$|\hat{f}(x) - \hat{f}(y)| \leq \|h\|_2 \|\delta\|_2 + \frac{1}{2} \|\delta\|_2 \|J\|_2 \|x + y\|_2.$$

Now $\|\delta\|_2 \leq \sqrt{d_H(x, y)}$ and $\|x + y\|_2 \leq 2\sqrt{m}$, which implies the bound. \square

This corollary directly motivates the spectral norm of J as a global diagnostic of landscape roughness. In particular, smaller $\|J\|_2$ implies smaller worst-case variation across the hypercube.

A.9 Ruggedness via Bit-Flip Variability

To study local ruggedness, we analyze the variability of single-bit moves over the hypercube.

Proposition (Exact second moment of bit-flip gains).

Assume x is drawn uniformly from $\{0, 1\}^m$. Then for each bit k ,

$$\mathbb{E}[\Delta_k(x)] = 0, \quad (24)$$

and

$$\mathbb{E}[\Delta_k(x)^2] = \left(h_k + \frac{1}{2} \sum_{\ell \neq k} J_{k\ell} \right)^2 + \frac{1}{4} \sum_{\ell \neq k} J_{k\ell}^2. \quad (25)$$

Proof. Using $\Delta_k(x) = (1 - 2x_k)g_k(x)$, note that $(1 - 2x_k)$ is independent of $g_k(x)$ and has mean zero and squared value one under the uniform measure. Hence,

$$\mathbb{E}[\Delta_k(x)] = \mathbb{E}[1 - 2x_k] \mathbb{E}[g_k(x)] = 0,$$

and,

$$\mathbb{E}[\Delta_k(x)^2] = \mathbb{E}[g_k(x)^2].$$

Since the coordinates $\{x_\ell\}_{\ell \neq k}$ are independent Bernoulli(1/2) variables,

$$\mathbb{E}[g_k(x)] = h_k + \frac{1}{2} \sum_{\ell \neq k} J_{k\ell}, \quad \text{Var}(g_k(x)) = \frac{1}{4} \sum_{\ell \neq k} J_{k\ell}^2.$$

The result follows from $\mathbb{E}[g_k(x)^2] = \text{Var}(g_k(x)) + \mathbb{E}[g_k(x)]^2$. \square

This proposition yields an exact measure of local ruggedness. We define the average ruggedness:

$$\mathcal{R}(J, h) = \frac{1}{m} \sum_{k=1}^m \mathbb{E}[\Delta_k(x)^2]. \quad (26)$$

When the latent bits are approximately balanced and the local fields are centered, the dominant contribution is:

$$\mathcal{R}(J, h) \approx \frac{1}{4m} \|J\|_F^2, \quad (27)$$

showing that interaction energy directly drives local variability. Thus, both $\|J\|_F$ and $\|J\|_2$ are theoretically meaningful diagnostics of ruggedness.

A.10 Low-Rank Structure and Effective Optimization Dimension

The spectral structure of J determines whether the landscape is effectively governed by a small number of collective directions. Let

$$J = \sum_{i=1}^m \lambda_i u_i u_i^\top \quad (28)$$

be the spectral decomposition of J , with eigenvalues ordered by decreasing magnitude:

$$|\lambda_1| \geq |\lambda_2| \geq \dots \geq |\lambda_m|.$$

For a given rank r , we define the truncated interaction matrix:

$$J_r = \sum_{i=1}^r \lambda_i u_i u_i^\top, \quad (29)$$

and the corresponding truncated objective:

$$\hat{f}_r(x) = h^\top x + \frac{1}{2} x^\top J_r x. \quad (30)$$

Proposition (Pointwise low-rank approximation). For every $x \in \{0, 1\}^m$,

$$|\hat{f}(x) - \hat{f}_r(x)| \leq \frac{m}{2} \|J - J_r\|_2. \quad (31)$$

Proof. We have:

$$\hat{f}(x) - \hat{f}_r(x) = \frac{1}{2} x^\top (J - J_r) x.$$

Therefore,

$$|\hat{f}(x) - \hat{f}_r(x)| \leq \frac{1}{2} \|J - J_r\|_2 \|x\|_2^2.$$

Since $x \in \{0, 1\}^m$, we have $\|x\|_2^2 \leq m$, which proves the result. \square

Corollary (Optimization gap under low-rank truncation). Let $x^* \in \arg \max_x \hat{f}(x)$ and $x_r^* \in \arg \max_x \hat{f}_r(x)$. Then,

$$\hat{f}(x^*) - \hat{f}(x_r^*) \leq m \|J - J_r\|_2. \quad (32)$$

Proof. From the previous proposition, $|\hat{f}(x) - \hat{f}_r(x)| \leq \varepsilon$ for all x , where $\varepsilon = \frac{m}{2} \|J - J_r\|_2$. Hence,

$$\hat{f}(x^*) \leq \hat{f}_r(x^*) + \varepsilon \leq \hat{f}_r(x_r^*) + \varepsilon \leq \hat{f}(x_r^*) + 2\varepsilon.$$

Substituting the value of ε yields the claim. \square

This corollary provides a concrete guarantee: if the spectral tail of J is small, then the optimization landscape is effectively low-dimensional, and the dominant eigenmodes of J capture most of the optimization-relevant structure.

A useful scalar summary of this concentration is the *effective rank*:

$$r_{\text{eff}}(J) = \frac{\|J\|_F^2}{\|J\|_2^2}, \quad (33)$$

which is small when interaction energy is concentrated in a few dominant modes.

A.11 Identifiability of the Learned QUBO Landscape

Let $\phi(x) \in \mathbb{R}^p$ denote the QUBO feature map containing all linear and pairwise terms, where

$$p = m + \frac{m(m-1)}{2}. \quad (34)$$

Let $\Phi(X) \in \mathbb{R}^{N \times p}$ be the design matrix formed from the observed latent codes in the training set.

Proposition (Non-identifiability under rank deficiency). If $\text{rank}(\Phi(X)) < p$, then the QUBO parameters are not uniquely identifiable from the observed data. In particular, there exists a nonzero vector $u \in \mathbb{R}^p$ such that:

$$\Phi(X)u = 0. \tag{35}$$

Therefore, for any parameter vector w , both w and $w + u$ induce identical predictions on all observed training codes, but can differ on unseen binary codes.

Proof. If $\text{rank}(\Phi(X)) < p$, then the null space of $\Phi(X)$ is nontrivial, so there exists $u \neq 0$ with $\Phi(X)u = 0$. Hence,

$$\Phi(X)(w + u) = \Phi(X)w,$$

so the two parameterizations agree on all observed codes. For an unseen code x with $\phi(x)^\top u \neq 0$, the predicted fitness differs:

$$\phi(x)^\top (w + u) \neq \phi(x)^\top w. \quad \square$$

Corollary (Dimension-sample trade-off). Since $p = O(m^2)$, increasing the latent dimension rapidly enlarges the number of QUBO parameters. When the number of observed sequences is not sufficiently large relative to p , the landscape away from the observed codes is only weakly constrained.

This result provides a formal explanation for the trade-off between latent dimensionality, surrogate generalization, and optimization stability. Ridge regularization selects one stable solution among many possibilities, but the induced landscape remains strongly dependent on the representation through the feature map $\Phi(X)$.

A.12 Why Prediction and Optimization Can Decouple

The previous results formalize why predictive accuracy alone does not determine optimization behavior.

First, predictive metrics such as Spearman correlation evaluate surrogate quality on a finite observed set, whereas optimization depends on the geometry of the entire hypercube. Second, our propositions show that when the QUBO feature map is rank-deficient or weakly constrained, multiple interaction structures can be consistent with essentially the same observed fit while differing away from the observed manifold.

Together, these observations imply that two latent representations can achieve similar predictive accuracy while inducing substantially different optimization landscapes. This representation-optimization decoupling is not an anomaly, but rather a structural consequence of learning a surrogate over a large discrete latent space.

A.13 Practical Consequences

The theory above yields several experimentally testable predictions. Landscapes with smaller $\|J\|_2$, faster spectral decay, and smaller ruggedness $\mathcal{R}(J, h)$ should be easier to optimize.

Likewise, increasing latent dimensionality without sufficient data should increase ambiguity in the learned landscape and make optimization less stable.

These further empirical analysis of the theory will be included in follow-up future works.

B Additional Experimental Details

B.1 Protein Sequence Embeddings (ESM)

We represent protein sequences using pretrained protein language models from the ESM family. In particular, we use the facebook/esm2_t6_8M_UR50D checkpoint from the Hugging Face Transformers library.

Given a protein sequence, we first convert it to uppercase and remove non-alphabetic characters. The cleaned sequence is then tokenized using the corresponding ESM tokenizer. We apply padding and truncation with a maximum sequence length of 1024.

The tokenized sequence is passed through the pretrained transformer model in evaluation mode without gradient computation. The model produces contextualized residue-level representations, from which we obtain a fixed-length sequence embedding by mean pooling over the sequence dimension using the attention mask:

$$e = \frac{\sum_{i=1}^L m_i H_i}{\sum_{i=1}^L m_i}, \tag{36}$$

where H_i denotes the hidden representation of the i -th residue and m_i is the corresponding attention mask.

Embeddings are computed in mini-batches of size 8 and stored as dense vectors in float32 format. These embeddings are used as inputs to downstream components, including the external fitness oracle and latent representation learning.

B.2 External Sequence-Level Fitness Oracle

For sequence-level fitness evaluation, we trained an external oracle on dense protein sequence embeddings. Each dataset was stored as a NumPy archive containing (i) dense embeddings, (ii) scalar fitness labels, and (iii) the corresponding protein sequences. The embeddings were represented in float32, while fitness targets were stored in float64.

Data splitting. We partitioned each dataset into training, validation, and test sets using a two-stage random split. First, we split the data into a training + validation set and a held-out test set with a test ratio of 0.2. Then, we further split the training + validation set into training and validation subsets using a validation ratio of 0.1 relative to the full dataset. This results in an effective split of 70%/10%/20% for training, validation, and test sets, respectively. All splits were performed with a fixed random seed of 42 for reproducibility.

Evaluation metrics. We evaluated model performance using four standard regression metrics: Spearman correlation, Pearson correlation, root mean squared error (RMSE), and mean absolute error (MAE). Metrics were reported on the training, validation, and test sets.

Models. We considered three regression models on top of the same embedding representation: Ridge Regression, XGBoost, and Gaussian Process Regression.

Ridge Regression. We used a pipeline consisting of feature standardization via `StandardScaler` followed by Ridge regression. The regularization strength was set to $\alpha = 1.0$, and the `svd` solver was used.

XGBoost. We used the `XGBRegressor` implementation with the following hyperparameters: number of trees = 300, maximum tree depth = 6, learning rate = 0.05, subsampling ratio = 0.9, column subsampling ratio = 0.9, ℓ_1 regularization coefficient = 0.0, and ℓ_2 regularization coefficient = 1.0. The objective function was squared error regression. Training was performed using 4 CPU threads, and the random seed was fixed to 42.

Gaussian Process Regression. We used a pipeline consisting of feature standardization followed by Gaussian Process Regression (GPR). The kernel was defined as:

$$k(x, x') = C \cdot \text{RBF}(x, x') + \text{WhiteKernel}, \quad (37)$$

where the constant kernel C was initialized to 1.0 with bounds $[10^{-3}, 10^3]$, the RBF kernel had an initial length scale of 1.0 with bounds $[10^{-3}, 10^3]$, and the white noise level was initialized to 10^{-3} with bounds $[10^{-6}, 10^1]$. The GPR model used `normalize_y=True` and performed 2 restarts of the optimizer.

Training protocol. All models were trained on both GFP and AAV datasets under four data regimes with training set sizes of $\{1000, 2000, 5000, 10000\}$. For each dataset and data regime, the same fixed hyperparameters and random seed were used. No additional hyperparameter search was performed. Models were trained on the training split and evaluated on validation and test splits.

Outputs. For each trained model, we stored (i) the serialized model parameters, (ii) evaluation metrics in JSON format, and (iii) test-set predictions including sequences, ground-truth fitness values, and predicted fitness values.

B.3 Latent Representation Learning and Decoder Implementation

We construct binary latent representations from dense ESM embeddings using four approaches: PCA, random projection, deterministic autoencoder (AE), and variational autoencoder (VAE). For all methods, we evaluate latent dimensions of 8, 16, 32, and 64.

For PCA, we apply principal component analysis to the dense embeddings and retain the top components corresponding to the target latent dimension. The resulting continuous representations are binarized using per-dimension median thresholding computed over the dataset. PCA-based binary representations are precomputed and reused across experiments.

For random projection, we project embeddings using a Gaussian random matrix with variance scaled by the input dimension, followed by the same median-based binarization. This provides a lightweight baseline without learned structure.

For AE and VAE, we use simple fully connected neural networks. The autoencoder consists of a two-layer encoder and decoder with a hidden dimension of 256 and ReLU activations. The encoder maps the input embedding to the latent space, and the decoder reconstructs the original embedding. The VAE uses a similar architecture with a shared encoder backbone and separate linear heads for the mean and log-variance. Both models are trained using mean squared reconstruction loss, with an additional KL divergence term for the VAE weighted by $\beta = 10^{-3}$. Latent representations are binarized by thresholding at zero.

Both AE and VAE are trained using the Adam optimizer with learning rate 10^{-3} , weight decay 10^{-5} , batch size 32, and 200 training epochs. All models are trained with a fixed random seed of 42 on CPU.

For decoding, we train a mutation-conditioned neural decoder that maps latent codes back to protein sequences. The decoder consists of two fully connected layers with hidden dimension 256 and ReLU activations, followed by two output heads: one for predicting mutation positions and one for predicting amino acid identities at mutated positions. The mutation prediction head outputs a vector of length equal to the sequence length, while the amino acid head outputs logits over 20 amino acids per position.

The decoder is trained using a combination of binary cross-entropy loss for mutation prediction and cross-entropy loss for amino acid prediction, with a higher weight assigned to the mutation loss to account for class imbalance. Training is performed using Adam with learning rate 10^{-3} , batch size 32, and 100 epochs. The best model is selected based on validation performance.

All latent models and decoders are trained across both GFP and AAV datasets and all data regimes using consistent hyperparameters.

B.4 Internal QUBO Surrogate Implementation

The internal surrogate operates directly on binary latent representations of dimension $m \in \{8, 16, 32, 64\}$ and models the fitness function as a combination of linear and pairwise interaction terms. Given a binary latent vector, the surrogate

includes all m linear terms and all $\frac{m(m-1)}{2}$ pairwise interaction terms. These features are constructed explicitly by concatenating the original binary variables with all pairwise products between distinct latent dimensions.

The model parameters are fitted using ridge regression with ℓ_2 regularization. Specifically, the surrogate is trained by solving a linear system involving the feature matrix and the target fitness values, with a regularization coefficient set to 10^{-3} . This closed-form solution enables efficient training even when the number of pairwise features grows quadratically with the latent dimension.

After training, the learned parameters are decomposed into a vector of linear coefficients and a symmetric matrix of pairwise interaction coefficients. The diagonal entries of the interaction matrix are set to zero, and symmetry is enforced by assigning equal weights to (i, j) and (j, i) . Predictions are computed by combining the linear contributions and pairwise interactions over the binary latent variables.

We evaluate the surrogate using standard regression metrics including RMSE, R^2 , and Spearman correlation on both training and held-out test sets. The model is trained using a fixed random seed of 42 and a train/test split ratio of 80/20.

For comparison, the implementation also includes a small multilayer perceptron (MLP) baseline trained using mini-batch gradient descent with ReLU activations. The MLP uses two hidden layers with dimensions 64 and 32, learning rate 10^{-3} , weight decay 10^{-5} , batch size 64, and 400 training epochs. However, this baseline is used only for reference, while all optimization experiments in the main paper rely on the QUBO surrogate.

The surrogate is trained across all dataset sizes and latent dimensions and serves as the objective function for downstream combinatorial optimization methods.

B.5 Combinatorial Optimization Methods

We optimize the learned QUBO surrogate in the binary latent space using five methods: Simulated Annealing (SA), Genetic Algorithm (GA), Random Search (RS), Greedy Hill Climbing (GHC), and a lightweight latent Bayesian optimization (LBO) baseline. All methods operate directly on binary vectors of dimension $m \in \{8, 16, 32, 64\}$.

Simulated Annealing (SA) starts from an initial binary code and iteratively proposes single-bit flips. At each step, a bit index is selected uniformly at random, and the energy change induced by flipping that bit is computed efficiently using the learned QUBO parameters. Moves that improve the objective are always accepted, while worse moves are accepted with a temperature-dependent probability. The temperature follows an exponential decay schedule with initial temperature $T_0 = 1.0$, minimum temperature 10^{-4} , and decay factor 0.999. The algorithm runs for 20,000 steps and keeps track of the best solution encountered during the trajectory.

The Genetic Algorithm (GA) maintains a population of candidate binary solutions and evolves them over multiple

generations. We use a population size of 64 and run the algorithm for 150 generations. At each generation, a subset of top-performing individuals (elite size 4) is preserved. New individuals are generated using tournament selection with tournament size 3, followed by single-point crossover applied with probability 0.9. Offspring are further perturbed using independent bit-flip mutation with mutation rate 0.02. The population is updated at each generation, and the best solution across all generations is returned.

Random Search (RS) samples binary latent codes independently and uniformly at random. We evaluate 10,000 candidate solutions and return the one with the highest objective value.

Greedy Hill Climbing (GHC) starts from an initial binary code and iteratively improves it by exhaustively evaluating all single-bit flips. At each iteration, the algorithm selects the bit flip that yields the largest improvement in the objective and updates the current solution accordingly. The process is repeated until no improving move exists or until a maximum of 100 passes over all bits is reached.

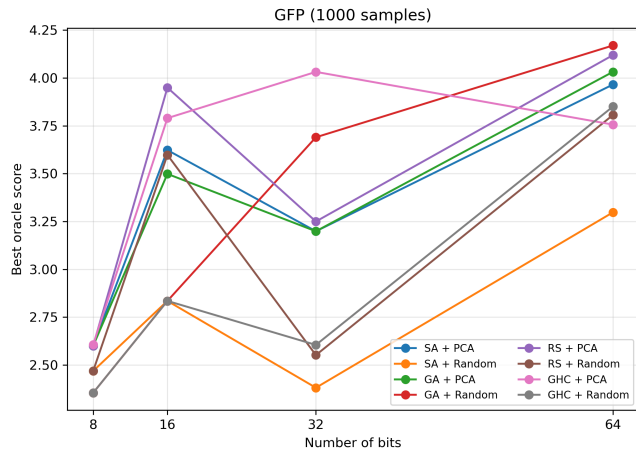
The Latent Bayesian Optimization (LBO) baseline uses a kernel-based uncertainty heuristic over binary latent codes. Given a set of seed solutions, the method samples 5,000 candidate binary vectors uniformly at random and evaluates an acquisition function based on an upper confidence bound. The predictive mean is computed using a kernel-weighted average over seed points, where the kernel is defined using an RBF function over Hamming distance with length scale 4.0. The acquisition function is given by the sum of the predictive mean and an exploration term weighted by $\beta = 1.0$. The candidate with the highest acquisition value is selected.

All optimization methods are applied consistently across datasets, latent dimensions, and data regimes using fixed hyperparameters.

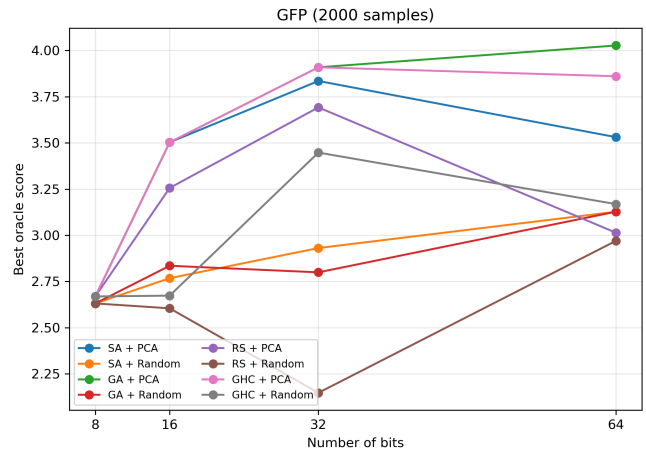
B.6 Additional Experimental Results

We provide detailed end-to-end design results across all dataset sizes and latent dimensions in Figures 5 and 6, as well as Tables 10–17. Figure 5 presents the performance trends on the GFP dataset across different training regimes, while Figure 6 shows the corresponding results for the AAV dataset. These figures illustrate how performance varies with latent dimensionality and optimization method. Tables 10–13 report detailed results for the GFP dataset at training sizes of 1000, 2000, 5000, and 10000 samples, respectively, while Tables 14–17 present the corresponding results for the AAV dataset across all data regimes. Each table includes both the best achieved score and the average performance of the top-10 candidates for each configuration, enabling a more fine-grained comparison across latent representations, optimization methods, and data regimes. Overall, these additional results further corroborate the trends observed in the main text, including the consistent advantage of PCA-based

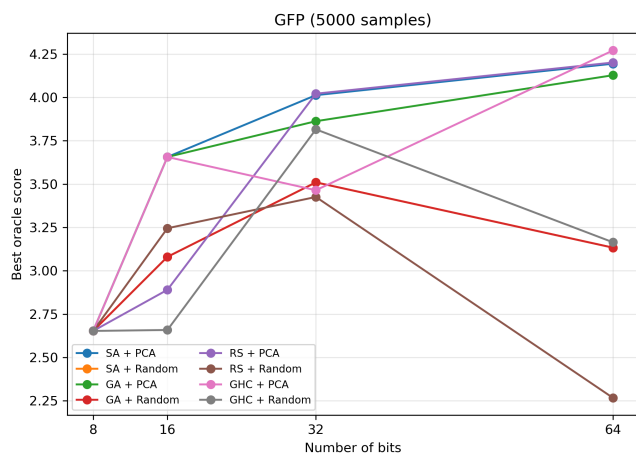
latent representations and the strong performance of combinatorial optimization methods such as greedy hill climbing, genetic algorithms, and simulated annealing.



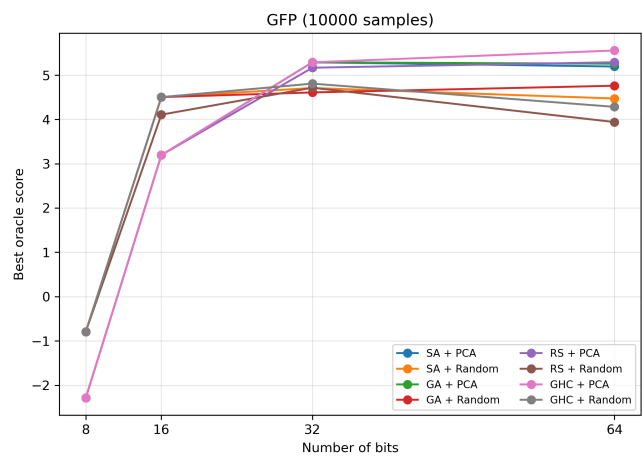
(a) GFP with 1000 training samples.



(b) GFP with 2000 training samples.



(c) GFP with 5000 training samples.



(d) GFP with 10000 training samples.

Figure 5. End-to-end design performance on GFP across different training sizes. The x-axis shows the number of bits and the y-axis shows the best oracle score. Each line corresponds to an optimizer-representation pair, including simulated annealing (SA), genetic algorithm (GA), random search (RS), and greedy hill climbing (GHC), combined with either PCA-based or random-projection binary latent representations.

Table 10. Detailed end-to-end design results on GFP with 1000 training samples.

Bits	Representation	Best optimizer	Best score \uparrow	Top-10 mean \uparrow
8	PCA	LBO	2.616	2.524
	Random	LBO	2.612	2.531
16	PCA	RS	3.950	3.247
	Random	RS	3.598	2.488
32	PCA	GHC	4.032	3.017
	Random	GA	3.690	2.525
64	PCA	RS	4.119	3.903
	Random	GA	4.170	3.312

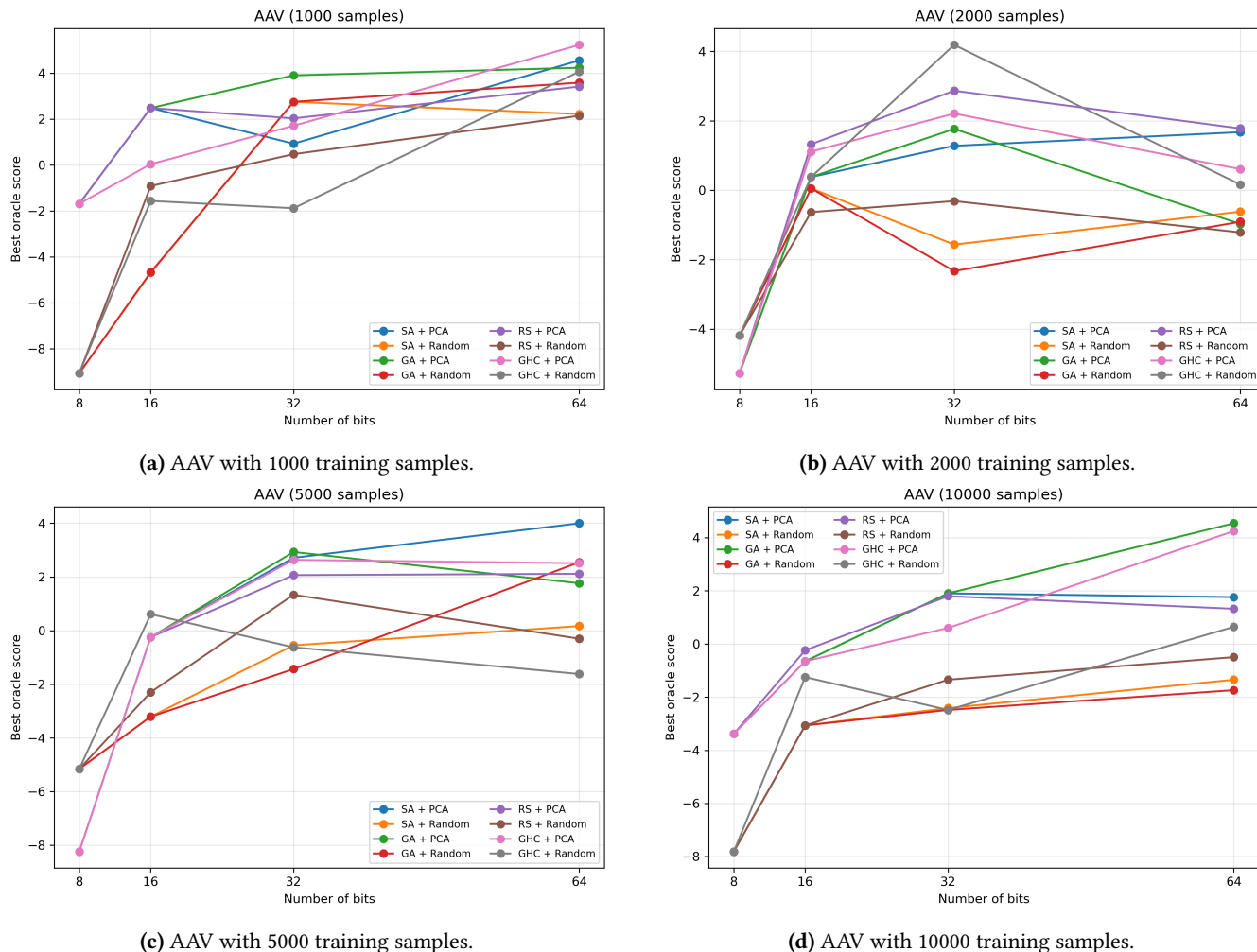


Figure 6. End-to-end design performance on AAV across different training sizes. The x-axis shows the number of bits and the y-axis shows the best oracle score. Each line corresponds to an optimizer-representation pair, including simulated annealing (SA), genetic algorithm (GA), random search (RS), and greedy hill climbing (GHC), combined with either PCA-based or random-projection binary latent representations.

Table 11. Detailed end-to-end design results on GFP with 2000 training samples.

Bits	Representation	Best optimizer	Best score \uparrow	Top-10 mean \uparrow
8	PCA	GA	2.669	2.669
	Random	LBO	2.669	2.267
16	PCA	GA	3.503	3.212
	Random	LBO	3.002	2.358
32	PCA	GA	3.909	3.449
	Random	GHC	3.448	2.693
64	PCA	GA	4.027	3.549
	Random	LBO	3.316	1.900

Table 12. Detailed end-to-end design results on GFP with 5000 training samples.

Bits	Representation	Best optimizer	Best score \uparrow	Top-10 mean \uparrow
8	PCA	GA	2.653	2.653
	Random	LBO	2.653	2.633
16	PCA	GHC	3.656	3.117
	Random	LBO	3.568	2.356
32	PCA	LBO	4.157	2.918
	Random	GHC	3.815	2.228
64	PCA	GHC	4.270	3.972
	Random	LBO	3.330	2.619

Table 13. Detailed end-to-end design results on GFP with 10000 training samples.

Bits	Representation	Best optimizer	Best score \uparrow	Top-10 mean \uparrow
8	PCA	LBO	3.162	-3.738
	Random	LBO	2.785	-4.556
16	PCA	LBO	4.712	3.452
	Random	GHC	4.502	3.029
32	PCA	GA	5.287	4.823
	Random	GHC	4.806	3.829
64	PCA	GHC	5.554	5.042
	Random	GA	4.758	3.003

Table 14. Detailed end-to-end design results on AAV with 1000 training samples.

Bits	Representation	Best optimizer	Best score \uparrow	Top-10 mean \uparrow
8	PCA	GA	-1.687	-4.039
	Random	LBO	-6.492	-7.534
16	PCA	SA	2.484	-1.568
	Random	RS	-0.913	-6.523
32	PCA	GA	3.906	-0.680
	Random	SA	2.753	-3.336
64	PCA	GHC	5.232	2.962
	Random	GHC	4.066	-1.557

Table 15. Detailed end-to-end design results on AAV with 2000 training samples.

Bits	Representation	Best optimizer	Best score \uparrow	Top-10 mean \uparrow
8	PCA	LBO	-4.213	-6.054
	Random	LBO	-3.352	-5.891
16	PCA	RS	1.325	-0.440
	Random	LBO	1.769	-3.162
32	PCA	RS	2.866	0.349
	Random	GHC	4.184	-2.674
64	PCA	RS	1.779	-0.353
	Random	GHC	0.164	-1.511

Table 16. Detailed end-to-end design results on AAV with 5000 training samples.

Bits	Representation	Best optimizer	Best score \uparrow	Top-10 mean \uparrow
8	PCA	LBO	-1.727	-6.113
	Random	LBO	-2.616	-5.168
16	PCA	RS	-0.245	-2.136
	Random	GHC	0.610	-2.630
32	PCA	GA	2.929	0.666
	Random	RS	1.336	-5.012
64	PCA	SA	3.999	2.249
	Random	GA	2.548	-1.150

Table 17. Detailed end-to-end design results on AAV with 10000 training samples.

Bits	Representation	Best optimizer	Best score \uparrow	Top-10 mean \uparrow
8	PCA	LBO	-1.903	-3.723
	Random	LBO	-5.172	-7.184
16	PCA	RS	-0.237	-2.834
	Random	LBO	1.197	-4.205
32	PCA	SA	1.904	0.727
	Random	LBO	-0.154	-5.185
64	PCA	GA	4.541	2.091
	Random	GHC	0.644	-2.174